Protective effect and molecular mechanisms of human non-neutralizing cross-reactive spike antibodies elicited by SARS-CoV-2 mRNA vaccination

Jordan Clark[1,2], Irene Hoxie[1,2] , Daniel C. Adelsberg[1], Iden A. Sapse[1], Robert Andreata-Santos[1,2,3], Jeremy S. Yong[1,2], Fatima Amanat[1], Johnstone Tcheou[1,2], Ariel Raskin[1,2], Gagandeep Singh[1,2], Irene González-Domínguez[1], Julia E. Edgar[4], Stylianos Bournazos[4], Weina Sun[1], Juan Manuel Carreño[1,2], Viviana Simon[1,2,5,6,7], Ali H. Ellebedy[8,9,10], Goran Bajic[1], and Florian Krammer[1,2,5]*

[1]*Department of Microbiology, Icahn School of Medicine at Mount Sinai, New York, NY, USA*

[2]*Center for Vaccine Research and Pandemic Preparedness (C-VARPP), Icahn School of Medicine at Mount Sinai, New York, NY, USA*

[3]*Retrovirology Laboratory, Department of Microbiology, Immunology and Parasitology, Paulista School of Medicine, Federal University of São Paulo (UNIFESP), São Paulo, SP, Brazil*

[4]*Laboratory of Molecular Genetics and Immunology, The Rockefeller University, New York, NY, USA*

[5]*Department of Pathology, Molecular and Cell Based Medicine, Icahn School of Medicine at Mount Sinai, New York, NY, USA*

[6]Division of Infectious Diseases, Department of Medicine, *Icahn School of Medicine at Mount Sinai, New York, NY, USA*

[7]The Global Health and Emerging Pathogens Institute, *Icahn School of Medicine at Mount Sinai, New York, NY, USA*

[8]*Department of Pathology and Immunology, Washington University School of Medicine, St. Louis, MO 63110, USA*

[9]*Center for Vaccines and Immunity to Microbial Pathogens, Washington University School of Medicine, St. Louis, MO 63110, USA*

[10]*The Andrew M. and Jane M. Bursky Center for Human Immunology and Immunotherapy Programs, Washington University School of Medicine, Saint Louis, MO 63110, USA*

*To whom correspondence should be addressed: florian.krammer@mssm.edu

Summary

Neutralizing antibodies correlate with protection against SARS-CoV-2. Recent studies, however, show that binding antibody titers, in the absence of robust neutralizing activity, also correlate with protection from disease progression. Non-neutralizing antibodies cannot directly protect from infection but may recruit effector cells thus contribute to the clearance of infected cells. Also, they often bind conserved epitopes across multiple variants. We characterized 42 human mAbs from COVID-19 vaccinated individuals. Most of these antibodies exhibited no neutralizing activity *in vitro* but several non-neutralizing antibodies protected against lethal challenge with SARS-CoV-2 in different animal models. A subset of those mAbs showed a clear dependence on Fc-mediated effector functions. We determined the structures of three non-neutralizing antibodies with two targeting the RBD, and one that targeting the SD1 region. Our data confirms the real-world observation in humans that non-neutralizing antibodies to SARS-CoV-2 can be protective.

42 **Introduction**

43 Severe acute respiratory syndrome coronavirus 2 (SARS-CoV-2) emerged in Wuhan, China in December
44 2019 and is the causative agent of the coronavirus disease 2019 (COVID-19) pandemic. As of November
45 2023, there have been over 6.9 million official deaths worldwide due to COVID-19 but the current estimate
46 based on excess mortality is as high as 27.3 million[1]. In late 2020, two mRNA-based vaccines, BNT162b2
47 (Pfizer) and mRNA-1273 (Moderna) received emergency use authorization from the United States Food
48 and Drug Administration (FDA) and by several countries worldwide in the following months. Numerous
49 additional vaccines based on different vaccine platforms are now available, including adenovirus-based
50 vectors, recombinant protein vaccines, DNA vaccines, and inactivated vaccines[2]. Most of these vaccines
51 utilize the spike glycoprotein of SARS-CoV-2 as an antigen, which is present on virions as a trimer. Spike
52 protomers are synthesized as single polypeptide chains which are subsequently cleaved into two subunits,
53 S1 and S2, by host proteases such as furin[3]. The receptor binding domain (RBD) within S1 interacts with
54 the angiotensin-converting enzyme 2 (ACE2) receptor, which is used by the virus to enter host cells[4].
55 Antibodies elicited against the spike, particularly against the RBD, can therefore prevent viral attachment
56 and neutralize the virus. However, neutralizing epitopes have also been reported within the spike
57 protein's S2 and N-terminal domains (NTD)[5–10]. While it has been shown that neutralizing titers correlate
58 with protection from COVID-19[11–14], the protective roles played by other non-neutralizing antibodies are
59 not well understood. Several reports have highlighted that vaccination elicits a larger number of non-
60 neutralizing antibodies than infection[15], and that despite the well-documented loss of neutralizing activity
61 against recently arisen variants of concern (VOCs), individuals vaccinated with the BNT162b2 and mRNA-
62 1273 vaccines still exhibit protection from disease[16]. Of note, Earle and colleagues found that binding
63 antibody titers alone correlate with protection[14], and a more recent study showed that binding antibodies
64 correlated with protection from progression to severe disease, even when neutralizing titers are
65 significantly reduced[17]. Taken together, these data suggest that other factors aside from neutralization
66 are important for the control and clearance of infection. Whilst non-neutralizing antibodies are unable to
67 prevent SARS-CoV-2 entry by binding virions via their fragment antibody binding (Fab) regions, their
68 fragment crystallizable (Fc) regions can still be engaged by the Fc gamma receptors (FcγRs) present on
69 various immune effector cell populations[18]. Interactions with these receptors can mediate protection via
70 antibody-dependent cellular cytotoxicity (ADCC)[19] and antibody-dependent phagocytosis (ADCP)[20], as well
71 as via modulation of antiviral CD8 T cell responses. Furthermore, the Fc regions can be recognized by the
72 complement component C1q[21]. This binding initiates the complement cascade and forms the membrane
73 attack complex (MAC), which can lyse infected cells and destroy virions[21]. ADCC is typically mediated by

natural killer (NK) cells[22], although monocytes and macrophages have also been implicated in this process[23], whereas ADCP is mediated by monocytes, macrophages, neutrophils, and eosinophils[20]. In a previous study, we identified 42 SARS-CoV-2 spike binding monoclonal antibodies (mAbs) derived from plasmablasts of three adults who had completed their primary BNT162b2 vaccination[15]. Of these, 12 bound RBD, 10 bound NTD, 17 bound S2, and three bound unknown epitopes. Interestingly, only seven mAbs (16%) were neutralizing. Several studies have highlighted the importance of effector cell-mediated immunity in protecting against SARS-CoV-2 infection[24–29]. Therefore, here we investigated whether these non-neutralizing antibodies could contribute to protection from SARS-CoV-2 infection in a lethal animal model and determined cryo-EM structures of selected mAbs to understand their molecular mechanism of action.

Results

Non-neutralizing antibodies maintain binding to divergent spike proteins

We previously cloned 42 monoclonal antibodies from the plasmablasts of three subjects who had received two doses of the Pfizer mRNA vaccine[10]. Due to the rapid evolution of immune evasive SARS-CoV-2 variants of concern (VOCs), the binding of these mAbs was tested against the spike proteins of the ancestral WA-1, Alpha (B.1.1.7), Beta (B.1.351), Delta (B.1.617.2), and the Omicron subvariants BA.5 and XBB.1. Many of the antibodies retained binding to the SARS-CoV-2 variants (Fig. 1A). Of the seven neutralizing mAbs tested, four NTD-binding mAbs exhibited reduced binding to the VOC spikes. Of these, PVI.V6-2 exhibited abrogated binding to Beta, BA.5, and XBB.1 spike, while PVI.V6-14[30] lost binding to BA.5 and XBB.1 spike. PVI.V5-6 and PVI.V6-7 maintained spike binding, however, the minimum binding concentration increased against all the tested VOCs. Of the two RBD-binding, neutralizing mAbs, PVI.V6-4 displayed reduced binding to BA.5 and XBB.1 spike, while PVI.V3-9 retained binding to each of the VOCs. Similarly, the NTD binding mAb PVI.6-11 bound strongly to all the VOC spikes. Conversely, binding was preserved for the majority of the non-neutralizing mAbs, with only four mAbs demonstrating a reduction in spike binding. To investigate whether the neutralizing antibodies that maintained binding to the VOCs could still neutralize, microneutralization assays were carried out using authentic ancestral, B.1.351, B.1.1617.2, BA.1, and BA.5 viruses. Regardless of spike binding, neutralization of the mAbs was abolished against all tested VOCs, except in the case of PVI.V6-4 and PVI.V3-9, which retained neutralization against Delta (Fig. 1B).

104 **Non-neutralizing antibodies protect from lethal challenge murine challenge and reduce lung viral titers**

105 To determine the protective abilities of the mAbs against SARS-CoV-2 infection, BALB/cAnNHsd mice were
106 treated intraperitoneally with 10mg/kg of antibody and infected intranasally with 5x the 50% lethal dose
107 (LD_{50}) of mouse-adapted SARS-CoV-2 (MA10)[31]. Of the RBD binding mAbs, the two neutralizing antibodies
108 were found to confer 100% survival, wherein animals treated with PVI.V6-4 lost no weight and animals
109 treated with PVI.V3-9 lost approximately 5% body weight (Fig. 2A). Three non-neutralizing mAbs (PVI.V3-
110 2, PVI.V6-3, and PVI.V6-12) were also found to confer 100% survival while two others (PVI.V3-16 and
111 PVI.V6-9) conferred 80% survival. Of the mAbs binding NTD, most of the neutralizing mAbs were found to
112 promote 100% survival with less than 5% weight loss (PVI.V-5-6, PVI.V6-2, PVI.V6-7, and PVI.V6-11) with
113 one mAb (PVI.V6-14) eliciting 60% protection with around 12% weight loss (Fig. 2B). One anti-NTD non-
114 neutralizing antibody (PVI.V5-2) promoted 100% survival with approximately 15% weight loss. Of the
115 mAbs cloned from the three mRNA recipients, the majority were found to be non-neutralizing antibodies
116 targeting S2. Of these, PVI.V5-1 conferred 100% survival with no weight loss, while three others (PVI.V3-
117 4, PVI.V3-13, and PVI.V6-6) elicited 80% survival; treatment with one mAb, PVI.V3-8, resulted in 60%
118 survival (Fig. 2C). Another antibody that binds a so far unknown epitope outside of the RBD, NTD, and S2
119 (PVI.V5-4), was also found to promote 100% survival following lethal challenge (Fig. 2D). In total, 19 of the
120 42 mAbs (45%) displayed protection from disease, with 12/19 (63%) of these being non-neutralizing mAbs.
121 To determine whether the protective non-neutralizing mAbs may be weakly neutralizing,
122 microneutralization assays were repeated using an increased mAb concentration of 200 µg/ml. These
123 assays identified mAb PVI.V6-3 as a weak neutralizer, with an IC50 of 98.86 µg/ml (Fig. S1). As the murine
124 challenge experiment was carried out using a dose of 10 mg/kg, the neutralizing effects of this mAb at the
125 *in vivo* available concentration are likely negligible.

126 To test these mAbs further using a severe model of SARS-CoV-2 infection, the transgenic hACE2-K18
127 mouse model was utilized with ancestral SARS-CoV-2. This mouse model expresses human ACE2,
128 rendering the mice highly susceptible to SARS-CoV-2 infection which progresses to fatal neurotropic
129 infection. We therefore tested whether the seven most protective mAbs (PVI.V5-1, PVI.V5-4, PVI.V6-2,
130 PVI.V6-3, PVI.V6-12, and PVI.V3-21) were able to confer protection when administered 2 hours prior to
131 infection with 3x and 5xLD_{50} doses of ancestral SARS-CoV-2. At a 3xLD_{50} infectious dose, the neutralizing
132 mAb PVI.V6-2, and the non-neutralizing mAb PVI.V5-1 promoted 100% survival, while PVI.V6-3 and
133 PVI.V6-12 promoted 80% and 60% survival respectively (Fig. S2). The non-neutralizing mAbs PVI.V5-2,
134 PVI.V5-4, PVI.V3-21 conferred 40% survival. At the 5xLD_{50} dose only PVI.V6-2 and PVI.V6-3 protected the

135 mice from challenge, with mice treated with the other non-neutralizing mAbs succumbing to infection by
136 8-10 dpi (Fig. S2). We then sought to validate the protective effects of these mAbs using a different model
137 which more closely recapitulates human disease. To this end, we tested whether PVI.V5-1, PVI.V5-4,
138 PVI.V6-2, PVI.V6-3, PVI.V6-12, and PVI.V3-21 were able to protect against ancestral SARS-CoV-2 challenge
139 in the Golden Syrian hamster model. Hamsters were treated intraperitoneally with 10mg/kg mAb 2 hours
140 prior to intranasal infection with wild-type SARS-CoV-2. Treatment with all mAbs, except for PVI.V5-4 and
141 PVI.V3-21, resulted in decreased weight loss compared to an irrelevant negative control mAb, indicating
142 that these mAbs can protect against wild-type SARS-CoV-2 infection in an alternative animal model with
143 wild-type virus (Fig. 2E).

144 To determine whether the 19 protective mAbs could reduce viral titers, mice were treated with 10mg/kg
145 of antibody, infected using a 1xLD_{50} dose of MA10 to prevent mortality, and lungs were harvested at 3-
146 and 5-days post-infection (dpi) for viral enumeration via plaque assay. At 3dpi all mAbs except for PVI.V5-
147 1, PVI.V5-2, PVI.V6-1, and PVI.V5-6 were found to significantly reduce lung viral titers (Fig. 3A-D). Mice
148 treated with the neutralizing antibodies PVI.V6-4, PVI.V3-9, and PVI.V6-11 exhibited no detectable virus
149 in their lungs whereas other neutralizing antibodies targeting NTD only moderately reduced viral titers.
150 The RBD, S2, and unknown epitope-binding, non-neutralizing mAbs were found to reduce viral titers
151 ranging from 10- to 1000-fold. At 5dpi all of the mAbs were found to significantly reduce viral titers with
152 the majority lowering titers below the limit of detection, indicating that both the neutralizing and non-
153 neutralizing mAbs promote viral clearance (Fig. 3E-H).

154

155 **Structural epitope mapping of non-neutralizing epitopes**

156 Given the protective potency of the non-neutralizing mAbs PVI.V5-4, PVI.V6-12, and PVI.V3-21, we wanted
157 to map their epitopes on spike to better understand the molecular mechanisms of protection. We
158 determined the cryo-EM structures of these mAbs (as Fabs to avoid cross-linking) in complex with a
159 prefusion SARS-CoV-2/human/USA/USA-WA1/2020 HexaPro spike (Fig. 4). We obtained modest-
160 resolution reconstruction for the PVI.V6-12 and PVI.V3-21 (Fig.4A, B) and a relatively high-resolution
161 reconstruction for the PVI.V5-4 (Fig.4C-E) complexes. The structures confirm that PVI.V6-12 and PVI.V3-
162 21 bind RBD; PVI.V6-12 most likely engages a complex epitope between two adjacent RBDs including the
163 360-370 α helix of one and the 500s loop of another RBD (Fig.4A). PVI.V6-12 likely does not discriminate
164 between the “up” or “down” RBD conformations, whereas PVI.V3-21 requires an open RBD (Fig.4B). In

165 fact, it appears that RBD is slightly dislodged "outward," away from the 3-fold axis of the spike trimer, in
166 our cryo-EM reconstruction, with PVI.V3-21 binding an epitope between the 340-helix and the 350-strand.
167 While we note that due to the Fab occupancy and the particle alignment issues, we could not resolve the
168 interaction interface on an individual amino acid level, for these two Fabs, we can conclude that both
169 PVI.V6-12 and PVI.V3-21 still likely allow for the spike ACE2 receptor engagement and therefore do not
170 neutralize the virus. Conversely, our 3.67Å resolution of the PVI.V5-4 Fab complex (Fig. 4C-E; S40) allowed
171 us to perform a more detailed structural analysis of this complex. First, we discovered that the unknown
172 epitope of PVI.V5-4 is the sub-domain 1 (SD1) within S1 (Fig. 4C), which is similar, but distinct from a
173 recently reported sd1.040[32]. Second, our structure shows that one Fab is bound to one spike trimer and
174 that the binding of PVI.V5-4 induces several structural rearrangements of the spike glycoprotein: (1) the
175 RBD of the Fab-bound protomer is dislodged slightly more outward, away from the 3-fold axis of the trimer
176 than in its canonically up conformation and (2) the Fab binding to one spike protomer likely induced the
177 dissociation of the adjacent S1 domain, as only two S1 domains are present in our structure – indeed, in
178 this conformation, PVI.V5-4 would sterically clash with the adjacent S1 NTD (Fig. S4). On the antibody side,
179 PVI.V5-4 engages SD1 with both the heavy and the light chains (Fig.4D). Loops 2 and 3 of the PVI.V5-4
180 heavy chain complementarity determining region (HCDR) are sandwiching the SD1 550-560 loop.
181 Additional intermolecular contacts are mediated by the LCDR3 loop (Fig.4D). The antibody HCDR3 Y111
182 and Y116, together with HCDR2 Y66 and LCDR3 Y92 amino acid side-chains, create an aromatic cradle that
183 accommodates the spike SD1 150-160 loop (Fig.4E). We speculate that PVI.V5-4 binding still allows for
184 ACE2 receptor engagement and hence does not neutralize the virus, but its epitope and angle of spike
185 engagement position it to effectively engage FcR and provide protection. Hence, PVI.V5-4 is functionally
186 distinct from sd1.040, which is a neutralizing mAb, by means of preventing ACE2-induced spike
187 conformational changes[32].

188

189 **Non-neutralizing mAbs can mediate ADCC, ADCP, and complement binding via interactions with their**
190 **Fc regions**

191 To determine whether the mAbs elicit protection via effector functions, ADCC and ADCP reporter assays
192 were performed using commercially available effector cells expressing either the human FcγRIIIa or
193 FcγRIIa receptors respectively. The majority of the 42 mAbs tested exhibited FcγRIIIa activity in a luciferase
194 reporter assay utilizing cells infected with recombinant Newcastle disease virus expressing the pre-fusion
195 wild-type spike (NDV-HexaPro-S)[33] (Fig. 5A). Neutralizing mAbs PVI.V3-9, PVI.V6-4, PVI.V6-2, PVI.V6-7, and

196 PVI.V6-11 exhibited the highest activity. Of the non-neutralizing RBD binding mAbs, PVI.V6-3 exhibited
197 the highest FcγRIIIa activity, while the protective mAbs PVI.V3-16, PVI.V3-21, PVI.V6-9, PVI.V6-12, and
198 PVI.V6-15 exhibited comparable activity (Fig. 5A). Notably, mAbs PVI.V3-18, PVI.V3-19, and PVI.V6-5,
199 which did not confer protection in the mouse challenge model, also demonstrated FcγRIIIa activity (Fig.
200 5A). For the NTD-binding mAbs, the protective mAb PVI.V6-8 exhibited FcγRIIIa activity, while the activity
201 of PVI.V5-2 was lower. The non-protective mAb, PVI.V3-15, displayed comparable activity to PVI.V6-8,
202 while mAbs PVI.V3-1 and PVI.V3-10 had little activity (Fig. 5A). The majority of the S2 binding mAbs
203 displayed comparable FcγRIIIa activity, despite only about 30% of these providing protection from lethal
204 challenge. Interestingly, the non-neutralizing mAbs PVI.V3-4, PVI.V5-2, and PVI.V5-4 did not display any
205 FcγRIIIa activity despite their ability to confer survival and reduce lung viral titers in the mouse challenge
206 experiments (Fig. 5A). Of the protective non-neutralizing mAbs, none demonstrated FcγRIIa activity,
207 however, all the neutralizing mAbs, except for PVI.V3-9 and PVI.V6-4, successfully induced reporter assay
208 responses (Fig. 5B). Overall, the majority of mAbs which were found to exhibit FcγRIIa binding activity
209 were those targeting NTD.

210 To determine if the mAbs can bind the components of the complement pathway, enzyme-linked
211 immunosorbent assays (ELISAs) were carried out in the presence of wild-type spike antigen, using
212 secondary antibodies specific to human C1q. Of the RBD binding mAbs, the neutralizing mAbs PVI.V3-9
213 and PVI.V6-4 exhibited the highest C1q binding, as did the non-neutralizing protective mAbs PVI.V3-21,
214 PVI.V6-3, PVI.V6-9, and PVI.V6-15 (Fig. 5C). Of the NTD binding, neutralizing mAbs, PVI.V6-11, PVI.V6-7
215 and PVI.V6-2 showed appreciable C1q binding, whereas PVI.V5-6 and PVI.V6-14 did not bind. Of the non-
216 neutralizing NTD binding mAbs, all except PVI.V3-10 bound C1q (Fig. 5C). For the S2 binding mAbs, the
217 protective, non-neutralizing mAbs PVI.V3-4, PVI.V6-1, and PVI.V6-10 displayed C1q binding, but PVI.V3-8,
218 PVI.V3-13, PVI.V5-1, and PVI.V6-6 showed little to no binding (Fig. 5C). The non-protective, non-
219 neutralizing mAbs PVI.V3-3, PVI.V3-5, and PVI.V3-6 also displayed appreciable C1q binding. Finally, the
220 protective SD-1 binding mAb PVI.V5-4 exhibited weak, but detectable C1q binding (Fig. 5C).

221 **Some non-neutralizing antibodies retain their protective capabilities in the absence of effector**
222 **functions**

223 To confirm that the mAbs elicit their protective effects via Fc interactions, a subset of 6 non-neutralizing
224 mAbs (PVI.V5-1, PVI.V5-2, PVI.V5-4, PVI.V6-3, PVI.V6-12, and PVI.V3-21) and one neutralizing mAb
225 (PVI.V6-2) which conferred 100% survival against lethal challenge were cloned into IgG1 expression
226 vectors that encode the LALA (L234A-L235A) or LALAPG (L234A-L235A, P329G) mutations[34,35]. The LALA

227 mutation diminishes Fc binding by the FcγRs on effector cells and by complement, while the additional PG
228 mutation abolishes all Fc binding[34,35]. ELISAs using ancestral SARS-CoV-2 spike confirmed that the binding
229 of the LALA and LALAPG mAbs was comparable to their wild type counterparts (Fig. S3). These "effector
230 silent" antibodies were utilized in ADCC/ADCP effector reporter assays in addition to C1q binding ELISAs.
231 As expected, the LALA and LALAPG mutant mAbs no longer displayed FcγRIIIa, FcγRIIa reporter activity or
232 C1q binding *in vitro* (Fig.6 A-C). The seven wild type mAbs were then employed in conjunction with their
233 LALA and LALAPG counterparts in a challenge study in which mice were treated intraperitoneally with
234 10mg/kg of mAb and then infected with a $5xLD_{50}$ dose of SARS-CoV-2 MA10. Unsurprisingly, the sole
235 neutralizing antibody, PVI.V6-2, maintained protection in the absence of effector functions at this
236 concentration (Fig. 6D). Both the LALA and LALAPG mutant PVI.V5-2 were unable to protect mice from
237 lethal challenge, with the mice succumbing to infection by 5dpi (Fig. 6D). The LALA and LALAPG mutant
238 PVI.V3-21 antibodies displayed increased weight loss and decreased survival. Similarly, the LALA and
239 LALAPG mutant PVI.V6-12 mAbs exhibited more weight loss than their wild-type counterpart, however
240 the LALA mutant still conferred 100% survival. The non-neutralizing mAb PVI.V6-3 exhibited increased
241 weight loss in the presence of the LALAPG mutations, however the LALA mutant mAb promoted
242 protection compared to wild-type. Surprisingly, antibodies PVI.V5-4 and PVI.V5-1 retained protection
243 even in the absence of effector functions. As these LALA and LALAPG mutant mAbs do not neutralize SARS-
244 CoV-2, and lack both effector cell and complement binding, the mechanism through which they promote
245 survival *in vivo* is unclear.

246 **Discussion**

247 Four years after its emergence, SARS-CoV-2 remains a serious threat to human health. With the continued
248 emergence of immune evasive SARS-CoV-2 VOCs that harbor spike mutations capable of ablating
249 neutralizing antibodies, the mechanisms that maintain protection without these responses require further
250 characterization. Numerous studies have shown that neutralizing antibodies elicited by vaccination
251 and/or infection correlate with protection from SARS-CoV-2 infection[12–14,36–39]. Conversely, a wealth of
252 literature that indicates that antibody functions other than direct neutralization also contribute to
253 protection from disease[40–49]. Additionally, several studies have shown that, while SARS-CoV-2 variants are
254 able to evade the neutralizing antibody response, conserved epitopes are still recognized by CD4+ and
255 $CD8^+$ T cells induced by both vaccination and infection[50–54]. In a previous study, we demonstrated that
256 SARS-CoV-2 elicits a higher proportion of non-neutralizing antibodies versus neutralizing antibodies,
257 predominantly against regions of the spike protein outside of the RBD[10]. To determine whether these

258 mAbs contribute to protection against SARS-CoV-2, we studied the ability of these mAbs to protect mice
259 from lethal challenge with mouse-adapted SARS-CoV-2. Seven of the 42 mAbs have previously been
260 demonstrated to neutralize the virus, while the remainder do not. As expected, all the neutralizing mAbs
261 protected mice against lethal challenge, however, with variable potency. Of the non-neutralizing mAbs,
262 19 promoted survival following lethal challenge, most of which were previously found to bind within the
263 RBD. While most of the tested mAbs bind within S2, only 5 of these were found to be protective. We
264 further validated the protective capabilities of these mAbs by testing the six most protective non-
265 neutralizing mAbs and one neutralizing mAb using the hamster and hACE2 K-18 challenge models. These
266 experiments confirmed that non-neutralizing mAbs can promote protection from challenge with ancestral
267 SARS-CoV-2, with some mAbs exhibiting comparable protection to neutralizing mAbs. Furthermore, these
268 mAbs showed protection even when tested using highly lethal challenge doses in animal models of SARS-
269 CoV-2 infection which display severe disease phenotypes. While these mAbs cannot block the virus, their
270 binding to cells which display spike on their surface resulted in the engagement of Fc-medicated ADCC in
271 a reporter assay.

272 During natural infection, the Fc portion of antibodies bound to virions and/or infected cells can interact
273 with the FcγRs of a diverse array of immune cells. The FcγRIIIa receptor is the sole FcγR expressed on NK
274 cells[50] that, when engaged, initiates a signaling cascade involving the phosphorylation of immunoreceptor
275 tyrosine-based inhibitory motifs (ITIMs)[55–58] thereby promoting ADCC activity. Similarly, the FcγRs
276 expressed on macrophages, monocytes, and granulocytes promote ADCP when interacting with the Fc
277 portions of antibodies bound to the viral glycoproteins present on virions and infected cells. Through these
278 mechanisms, non-neutralizing antibodies can promote the clearance of virions and infected cells and, as
279 a result, curtail infection and reduce viral loads in infected tissues. The Fc regions of antibodies bound to
280 free virions can also be engaged by C1q, the first protein involved in the classical complement cascade.
281 The complement system is composed of over 30 heat-liable proteins that are present within plasma[21,59–
282 61]. The engagement of the Fc region of antibodies by Cq1 initiates an enzymatic cascade which generates
283 the membrane attack complex (MAC), a pore-forming complex that ruptures lipid bilayers. Importantly,
284 the MAC can form on infected cells and virus particles, providing a mechanism through which virus-
285 producing cells and free virions can be destroyed.

286 Most of the non-neutralizing mAbs described herein can engage both effector cells and C1q via their Fc
287 domains, indicating that this is likely the mechanism through which they protect mice from lethal
288 challenge. Indeed, at 3 dpi, the neutralizing mAbs targeting the RBD had effectively reduced viral loads

289 below the limit of detection, whereas the non-neutralizing antibodies reduced loads to a lesser, but still
290 significant extent. Of the five NTD-binding neutralizing mAbs, only PVI.V6-11 reduced viral loads below
291 the limit of detection at 3dpi, however PVI.V6-2 and PVI.V6-7 both promoted protection from lethal
292 infection despite maintaining high lung titers. The mice treated with the majority of the non-neutralizing
293 mAbs exhibited increased weight loss and lung viral loads compared to those treated with neutralizing
294 mAbs, demonstrating that non-neutralizing mAbs are less efficient at restricting viral infection. Given that
295 neutralizing mAbs are capable of inactivating free virions, and non-neutralizing mAbs predominantly work
296 upon infected cells, these results indicate that non-neutralizing antibodies can still elicit effective
297 protection from disease, however not to the same extent as neutralizing antibodies – and from a
298 mechanistic perspective they cannot protect from infection. Conversely, as the majority of non-
299 neutralizing mAbs tested here retain binding to variant SARS-CoV-2 spikes, the effector functions may
300 help ameliorate disease burden upon infection with SARS-CoV-2 VOCs.

301 To test whether the most protective non-neutralizing antibodies restrict viral infection via Fc medicated
302 interactions, six of the non-neutralizing mAbs which conferred 100% survival against lethal challenge were
303 cloned into expression vectors harboring the LALA or LALAPG mutations in their Fc regions[62,63]. One
304 protective, RBD-binding, neutralizing mAb, PVI.V6-2, was also mutagenized as a control. These mutations
305 have been used extensively in previous research wherein mAbs have been developed for therapeutic
306 use[34,35,63–66]. ADCC and ADCP effector cell reporter assays and complement ELISAs confirmed that the
307 inclusion of both the LALA and LALAPG mutations abrogated the effector functions of these mAbs. When
308 this panel of mAbs was investigated in the mouse challenge model, as expected, the neutralizing mAb
309 PVI.V6-2 retained 100% protection, even in the presence of the LALA and LALAPG mutations. While
310 neutralizing mAbs can also engage effector cells and complement, the neutralization of virus is the most
311 likely mechanism through which this mAb protects against infection. Conversely, both the LALA and
312 LALAPG counterparts of the non-neutralizing mAb PVI.V5-2 no longer protected mice from infection,
313 indicating that it likely interacts predominantly with effector cells to promote ADCC and ADCP. Similarly,
314 the non-neutralizing mAb PVI.V3-21 LALA mutant elicited 50% protection, whereas the LALAPG mutant
315 provided 20% protection. This indicates that this mAb likely engages both complement and effector cells.
316 The non-neutralizing mAb PVI.V6-12 lost all protective capabilities following LALAPG mutagenesis,
317 however provided 100% protection from infection with only LALA. Surprisingly, the non-neutralizing
318 antibodies PVI.V5-1, PVI.V6-3, and PVI.V5-4 retained protection even when mutagenized to include the
319 LALA and LALAPG substitutions. PVI.V6-3 exhibited weak *in vitro* neutralizing activity and is likely incapable
320 of neutralizing virus at the 10 mg/kg dose used, however this activity may explain some of its protective

321 effects in the presence of the LALA and LALAPG mutations. As PVI.V5-1 and PVI.V5-4 are unable to
322 neutralize and, when mutagenized, longer engage effector cells or complement, the mechanism through
323 which they induce protection from infection is unclear. It has previously been reported that non-
324 neutralizing Ebola virus mAbs, mutagenized with the G236R/L328R mutation which abrogates Fc binding,
325 retained protection in a mouse challenge model[67]. This indicates that the mechanisms through which
326 these mAbs inhibit virus cannot be recapitulated using *in vitro* neutralization assays and can only be
327 probed using animal models.

328 Structural epitope mapping can provide invaluable information about the molecular mechanisms of
329 antibody protection. We used single-particle cryo-EM to glean insights into how non-neutralizing
330 antibodies protect by virtue of engaging the spike on infected cells, activating phagocytic and cytolytic
331 cells and thus helping reduce the disease burden in infected individuals. We showed that PVI.V3-21,
332 PVI.V5-4, and PVI.V6-12 bind epitopes that do not interfere with the spike cellular receptor ACE2 binding
333 but potentially position their Fc portion for efficient activation of effector functions like ADCC, ADCP, and
334 complement activation. Notably, we also report on a detailed structural characterization of a non-
335 neutralizing human antibody that targets SD1, a vastly underappreciated yet conserved domain on spike
336 adjacent to RBD. Previous studies have shown that interactions between the RBD and SD1 of one spike S1
337 protomer and the NTD of the neighboring S1 protomer can stabilize the spike in its prefusion
338 conformation[68]. Our structure of PVI.V5-4 bound to SD1 shows that antibodies that engage SD1 destabilize
339 those protomer-protomer interactions and dislodge the neighboring NTD. Thus, while PVI.5-4 is devoid of
340 neutralizing and effector functions, it does prevent weight loss in a murine model of infection, probably
341 by destabilizing the spike quaternary architecture on infected cells. While PVI.5-4 showed no neutralizing
342 activity in our *in vitro* assays, other SD1-targeting antibodies have been shown to neutralize the virus by
343 inhibiting the conformational changes that would expose the S2 fusion loops upon ACE2 receptor
344 engagement[32]. We believe that SD1-targeting antibodies could be a valuable component of the humoral
345 response against SARS-CoV-2 and other coronaviruses. Questions remain about their prevalence in
346 infection- and vaccination-induced humoral immunity.

347 Taken together, these results suggest that non-neutralizing antibodies play important roles in the
348 protecting against COVID-19, that such mAbs may provide protection against emerging variants and, if
349 sufficiently cross-reactive, perhaps against other betacoronaviruses[69]. Critically, while some non-
350 neutralizing SARS-CoV-2 mAbs have been reported to exhibit antibody-dependent enhancement (ADE) *in*
351 *vitro*[70–73], our study and others demonstrate a lack of ADE *in vivo*[72] indicating that mAbs with no

352 neutralizing activity do not promote enhanced disease phenotypes. Finally, our findings are in line with
353 reports that show binding antibody levels correlation with protection from severe outcomes in humans
354 in the absence of robust neutralizing activity[17].

355 **Limitations of the study**

356 Some important caveats of this work should be considered. As we have performed effector cell reporter
357 assays using recombinant cells which express either hFcγRIIIA or hFcγRIIA receptors, we are unable to
358 model the complex expression pattern of these receptors which are present together on some immune
359 cell populations and function in conjunction with the inhibitory receptor FcγRIIB. Additionally, there are
360 important differences between the human and murine FcγRs, wherein mice express four different, but
361 homologous receptors (mFcγRI, mFcγRIIB, mFcγRIII and mFcγRIV). Despite these complexities, human IgG
362 can bind orthologous murine and hamster FcγRs with similar affinity to their human counterparts[74,75],
363 however mice do not recapitulate the diversity or expression patterns of the human FcγRs[76]. In future
364 studies, these differences could be overcome by using humanized mice which express the human FcγRs[77].
365 Additionally, we have performed challenge studies using a single 10 mg/kg dose of mAb; differences in
366 weight loss and survival may be more obvious when utilizing de-escalating doses.

367

368 **Material and methods**

369 **Cells and viruses**

370 Vero.E6 cells (American Type Culture Collection, ATCC, CRL-1586, clone E6) were maintained in Dulbecco's
371 modified Eagle medium (DMEM; Gibco), supplemented with Antibiotic-Antimycotic (100 U/mL penicillin–
372 100 µg/mL streptomycin–0.25 µg/mL amphotericin B; Gibco), and 10% fetal bovine serum (FBS; Corning)
373 in a 37°C incubator with 5% CO_2. Vero.E6 cells expressing Transmembrane protease, serine 2 (TMPRSS2,
374 BPS Biosciences, 78081) were cultured in Dulbecco's modified Eagle medium (DMEM; Gibco)
375 supplemented with 10% FBS, 1% minimum essential medium (MEM) amino acids solution (Gibco, cat. no.
376 11130051), 100 U ml−1 penicillin and 100 µg mL−1 streptomycin (Gibco, cat. no. 15140122), 100 µg mL−1
377 normocin (InvivoGen, cat. no. ant-nr), and 3 µg mL−1 puromycin (InvivoGen, cat. no. ant-pr). Expi293F
378 cells were maintained in Expi293 media in a shaking incubator at 37°C and 8% CO_2.

379 Mouse-adapted SARS-CoV-2 (SARS-CoV-2 MA10, BEI Resources NR-55329), wild-type SARS-CoV-2 (isolate
380 USA-WA1/2020), and Beta SARS-CoV-2 (B.1.351, hCoV-19/South Africa/ KRISP-K005325/2020, BEI
381 Resources NR-54009), were obtained from BEI Resources. SARS-CoV-2 BA.1 (B.1.1.529, USA/NY-MSHSPSP-
382 PV44488/2021, EPI_ISL_7908059) and SARS-CoV-2 BA.5 USA/NY-MSHSPSP-PV58128/2022 have been
383 described previously[78]. Wild-type SARS-CoV-2 and SARS-CoV-2 MA10 were grown in Vero.E6 cells whereas
384 Beta, Delta, BA.1, and BA.5 SARS-CoV-2 were grown using Vero.E6 TMPRSS2 cells. All viruses were grown
385 for 3 days at 37°C prior to clarification via centrifugation at 1,000g for 10 minutes. Viral stocks used were
386 sequence-verified and tittered using both the 50% tissue culture infectious dose ($TCID_{50}$) method and via
387 plaque assay on Vero.E6 TMPRSS2 cells before use in microneutralization assays and challenge
388 experiments. Virus stocks were stored at −80°C before use. All experiments with authentic replication
389 competent SARS-CoV-2 were performed in the biosafety level 3 (BSL-3) facility following institutional
390 guidelines.

391 **Recombinant protein production**

392 Recombinant proteins were expressed in Expi293F cells (Life technologies). Full-length spike proteins were
393 cloned into the pCAGGS mammalian expression vector as previously described[79,80]. MAbs were also
394 produced via the transfection of expression vectors encoding the mAb heavy chain and light chains as
395 previously described[10]. Cells were grown to $3x10^6$ cells/mL and transfected using Expifectamine (Life
396 Technologies) with 1 µg of plasmid per mL of culture media, as per manufacturer's instructions. Enhancer
397 solutions were added 24 hours post-transfection and cells were allowed to incubate for 3 days. At this

398 point, the supernatant was removed, clarified by centrifugation at 4,000 g for 30 mins, and filtered using
399 0.45 µM Stericup filters (Sigma-Aldrich). Proteins were purified from filtered supernatants using nickel
400 nitriloacetic acid (Ni-NTA) agarose (QIAGEN) via gravity flow, and proteins were eluted in line with
401 previous publications[10]. Eluted proteins were buffer exchanged using 50 kDa Amicon centrifugal units
402 (EMD Millipore), resuspended in phosphate-buffered saline (PBS), and quantified using a Bradford assay
403 (Bio-Rad). Human IgG1 expression vectors harboring the LALA and LALAPG mutations were kindly
404 provided by Ali Ellebedy. The VH genes of PVI.V3-21, PVI.V5-1, PVI.V5-2, PVI.V5-4, PVI.V6-2, PVI.V6-3, and
405 PVI.V-12 were amplified via PCR and cloned into the LALA and LALAPG IgG1 vectors using InFusion cloning
406 (Takara).

407 **ELISA**

408 Recombinant proteins were coated on Immulon 4 HBX 96-well plates (Thermo Scientific) at a
409 concentration of 2 µg/mL in PBS, 50 µL per well overnight at 4°C. 24 hours later, the coating solution was
410 removed, and plates were blocked with 3% non-fat milk (Life Technologies) diluted in PBS containing
411 0.01% Tween-20 (PBST; Fisher Scientific). Plates were incubated with the blocking solution for 1 hour prior
412 to 3 washes using PBST. MAbs were serially diluted 1:10 from a starting concentration of 30 µg/mL in PBST
413 supplemented with 1% non-fat milk and were added to the respective plates. Primary antibody was not
414 added to 16 wells per ELISA plate to serve as blank. After a 1-hour incubation at room temperature, the
415 plates were washed 3 times with PBST and 100 µL of mouse anti-human IgG conjugated to horseradish
416 peroxidase (HRP) diluted 1:3000 in PBST supplemented with 1% non-fat milk was added to each well. After
417 an incubation time of 1 hour at room temperature, plates were again washed three times with PBST prior
418 to the addition of 100 µL of o-phenylenediamine dihydrochloride (Sigma-Aldrich; OPD). Plates were
419 allowed to develop for 10 minutes after which the reaction was stopped via the addition of 50 µL of 3M
420 hydrochloric acid (HCl). The plates were read using a Synergy 4 (BioTek) plate reader at an optical density
421 of 490 nanometers. The area under the curve (AUC) and the minimal binding concentrations for each plate
422 was calculated using GraphPad Prism 10, with the average plus 5 standard deviations of the blank wells
423 serving as the baseline. C1q and C3 binding ELISAs were carried out as previously described. Briefly, mAbs
424 were diluted to 100 µg/mL and serially diluted 1:3 in sterile PBS. 50 µL of these dilutions were utilized to
425 coat Immulon 4 HBX 96-well plates (Thermo Scientific) overnight at 4°C. The plates were then washed
426 three times with PBST and blocked using 100 µL of protein-free blocking buffer (Pierce) per well for 1
427 hour. Human serum was then diluted to 3% (vol/vol) in protein-free blocking buffer (Pierce), and 100 µL
428 was incubated per well for 1 hour. Following an additional three PBST washes, 100 µL of biotinylated anti-

429 human C1q (ab48341, Abcam) or anti-human C3 (ab48342, Abcam), diluted 1:3000 in protein-free
430 blocking buffer was added to each well and incubated for 1 hour at room temperature. Following three
431 PBST washes, 100 µL of high sensitivity streptavidin conjugated to HRP (Thermofisher) diluted 1:3000 in
432 protein-free blocking buffer was added. The plates were developed using an identical method to the
433 conventional ELISA, and the data was analyzed using GraphPad Prism 10.

434 **Microneutralization assays**

435 All work with SARS-CoV-2 was performed in a biosafety level 3 (BSL3) laboratory. Vero.E6 TMPRSS2 cells
436 were seeded in a 96-well cell culture plate (Corning; 3340) at a density of $1x10^4$ cells per well. MAb
437 dilutions were prepared in 1× minimal essential medium (MEM; Gibco) supplemented with 2% FBS. The
438 irrelevant influenza A (IAV) antibody, CR9114, was included as a negative control[48] . 24 hours later cells
439 were infected with 10^4 tissue culture infectious dose 50 ($TCID_{50}$)/mL, and 80 µL of virus and 80 µL of
440 antibody dilution were combined and incubated together for 1 hour at room temperature on a separate
441 96-well plate. After the incubation, 120 µL of virus–antibody inoculum was utilized to infect cells for 1
442 hour at 37°C. After one hour, the inoculum was removed and 100 µL of each corresponding dilution was
443 added to the wells. A volume of 100 µL of 1X MEM was also added to the plates to achieve a total volume
444 of 200 µL per well. Cells were incubated at 37°C in a 5% CO_2 incubator for 3 days and fixed with 10%
445 paraformaldehyde (Polysciences) for 24 hours. The paraformaldehyde was removed, and cells were
446 washed twice with PBS prior to permeabilization by the addition of 150 µL of 0.1% Triton X-100 (Fisher
447 followed by incubation at room temperature for 15 minutes. The Triton X-100 solution was removed, cells
448 were blocked with PBS supplemented with 3% non-fat milk (American Bio; catalog no. AB10109-01000)
449 for one hour, and then stained using the anti-nucleoprotein antibody 1C7 as previously described[81].

450 **ADCC and ADCP *in vitro* reporter assays**

451 Vero.E6 cells (ref) were seeded in 96 well plates (Corning; 3340) at a seeding density of $2x10^4$ cells per well
452 24 hours prior to infection with NDV-HexaPro-S[82] at a multiplicity of infection (MOI) of 2. One hour later
453 the inoculum was removed and replaced with 100µl of Roswell Park Memorial Institute (RPMI-1640)
454 media (Thermofisher). 48 hours later the media was removed and replaced with 25 µL of RMPI-1640
455 media supplemented with 2% low-IgG FBS (Promega). Antibodies were serially diluted 1:10 in RPMI 1640
456 media from a starting concentration of 30 µg/mL to a final concentration of 0.014 µg/mL and 25 µL of
457 antibody dilution was added to the plate. CR9114 was utilized as a negative control[48]. MAb dilutions were
458 not added to 16 wells per plate to provide background luminescence readings. $3x10^6$ ADCC and ADCP

459 Bioassay Effector Cells expressing the human FcγRIIIa or FcγRIIa receptors (Promega) were added per well
460 and the cells were incubated in at 37°C with 5% CO_2 for 6 hours. 75 µL of Bio-Glo luciferase reagent
461 (Promega) was then added to each well and the luminescence was read in a Synergy 4 (BioTek) plate
462 reader. The background luminescence reading was used to calculate AUC using GraphPad Prism 10.

463 ***In vivo* studies**

464 All animal procedures were performed by following the Institutional Animal Care and Use Committee
465 (IACUC) guidelines of the Icahn School of Medicine at Mount Sinai IACUC and according to an approved
466 protocol. To determine the LD_{50} of SARS-CoV-2 MA10, 6- to 8-week-old female, BALB/cAnNHsd mice
467 (Envigo) were infected with serial dilutions of the virus ranging from 10^5 to 5 plaque forming units (PFU).
468 LD50 experiments were carried out identically in the hACE2 K-18 mice using SARS-CoV-
469 2/human/USA/USA-WA1/2020. For antibody protection studies, 6–8-week-old female BALB/cAnNHsd or
470 B6.Cg-Tg(K18-ACE2)2Prlmn/J mice (The Jackson Laboratory) were treated intraperitoneally with 10 mg/kg
471 of antibody diluted in sterile PBS. Two hours post-treatment mice were administered anesthesia
472 intraperitoneally (IP) and intranasally (IN) infected with 50 µL of either $1xLD_{50}$ or $5xLD_{50}$ of SARS-CoV-2
473 MA10 or WA1/2020 diluted in sterile PBS. Anesthesia was prepared using 0.15 mg/kg ketamine and 0.03
474 mg/kg xylazine in water for injection (WFI; Gibco). Weights were recorded over a period of 1-2 weeks and
475 mice falling below 75% of their original body weight were humanely sacrificed via cervical dislocation.
476 When assessing lung viral loads, mice were humanely sacrificed on days 3- and 5-dpi for enumeration of
477 virus in the lungs. Lungs were homogenized using a BeadBlaster 24 (Benchmark) homogenizer and
478 clarified by centrifugation at 1,000 g for 10 minutes at 4°C. Viral load in the lung was quantified via a classic
479 plaque assay. For the hamster studies, 6-8-week-old female Syrian hamsters (Envigo) were treated
480 intraperitoneally with 10 mg/kg of antibody diluted in sterile PBS. Two hours later, hamsters were
481 anesthetized via the IP administration of 50-200 mg/kg ketamine and 5-10 mg/kg xylazine and infected IN
482 with 100 µL sterile PBS containing 10^5 PFU of wild-type SARS-CoV-2 (isolate USA-WA1/2020). Weight loss
483 was recorded for 10 days. The IAV mAb, CR9114, was included as a negative control in all animal studies[48].

484 **Cryo-EM sample preparation and data collection**

485 SARS-CoV-2 HexaPro Spike[83] was incubated with PVI.V3-21, PVI.V5-4, or PVI.V6-12 Fabs at 2 mg/mL and a
486 molar ratio of 1.2:1 Fab:Spike for 20 minutes at 4°C. Immediately before grid preparation, fluorinated
487 octyl maltoside was added to the pre-formed complex at 0.02% w/v final concentration. Then, 3 µL
488 aliquots were applied to UltrAuFoil gold R0.6/1 grids (Quantifoil) and subsequently blotted for 6 seconds

489 at blot force 0, then plunge-frozen in liquid ethane using an FEI Vitrobot Mark IV. Grids were imaged on a
490 Titan Krios microscope operated at 300 kV and equipped with a Gatan K3 Summit direct detector. 5,894
491 movies were collected in counting mode at a total dose of 52.51 $e^-/Å^2$ at a magnification of 81,000,
492 corresponding to a calibrated pixel size of 1.069 Å. Defocus values were from -0.5 to -1.5 µm.

493 **Cryo-EM data processing**

494 Movies were aligned and dose weighted using MotionCorr2[84]. Contrast transfer function estimation was
495 done in cryoSPARC v3.3.1[85] using CTFFIND4 and particles were picked with cryoSPARC's blob picker. The
496 picked particles were extracted with a box size of 512 pixels, with 4x binning and subjected to a 2D
497 classification. Selected particles were then subjected to a second round of 2D classification. An initial
498 model was generated on the 951,973 selected particles at 6 Å/pixel. After one round of non-uniform
499 refinement, without imposed symmetry, the particles were subjected to 3D classification with 10 classes.
500 Of these, the best 3 classes, containing 173,783 particles in total, were combined, re-extracted without
501 binning with a box size of 512 pixels, and selected for further rounds of non-uniform refinement with local
502 CTF refinement, yielding the final global map at a nominal resolution of 3.35 Å. The protomer with the
503 Fab volume was subjected to local refinement with a soft mask extended by 6 pixels and padded by 12
504 pixels encompassing the RBD, SD1, and Fab. This yielded the final local map at 3.67 Å resolution. The two
505 half-maps from the global or local refinement were used for sharpening in DeepEMhancer (PMID:
506 34267316) The reported resolutions are based on the gold-standard Fourier shell correlation of 0.143
507 criterion.

508 **Model building and refinement**

509 Spike from PDB ID: 6ZGE and SAbPred[86] generated Fab variable domains were fit into the focus refined
510 map using UCSF ChimeraX[87] and then manually built using COOT[88]. N-linked glycans were built manually
511 in COOT using the glyco extension and their stereochemistry and fit to the map validated with Privateer[89].
512 The model was then refined in Phenix[90] using real-space refinement and validated with MolProbity[91]. The
513 structural biology software was compiled and distributed by SBGrid[92].

514 **Data availability**

515 The atomic models and corresponding maps are available online under the following accession codes. For
516 the PVI.V5-4 complex, the atomic model is available in the Protein Data Bank (PDB) under accession code
517 8VIA. The cryo-EM maps and the raw micrographs are available in the Electron Microscopy Data Bank
518 (EMDB) and in the Electron Microscopy Public Image Archive (EMPIAR) under accession codes EMD-43255

519 and EMPIAR-11847, respectively. Additionally, cryo-EM maps for the PVI.V3-21 and PVI.V6-12 complexes
520 have been deposited to EMDB under accession codes EMD-43306 and EMD-43314, respectively. All other
521 data underlying figures in this paper can be found in ImmPort under identifier xxx.

522

523 **Acknowledgments**

524 We thank the Mount Sinai Pathogen Surveillance Program for providing representative SARS-CoV-2 viral
525 isolates.

526 G.B. was in part supported by NIH R01AI168178 and the Irma T. Hirschl/Monique Weill-Caulier Trust.

527 Some of this work was performed at the National Center for CryoEM Access and Training (NCCAT) and the
528 Simons Electron Microscopy Center located at the New York Structural Biology Center, supported by the
529 NIH Common Fund Transformative High Resolution Cryo-Electron Microscopy program (U24 GM129539),
530 and by grants from the Simons Foundation (SF349247) and NY State Assembly.

531 This effort was supported by the Serological Sciences Network (SeroNet) in part with Federal funds from
532 the National Cancer Institute, National Institutes of Health, under Contract No. 75N91019D00024, Task
533 Order No. 75N91021F00001. The content of this publication does not necessarily reflect the views or
534 policies of the Department of Health and Human Services, nor does mention of trade names, commercial
535 products or organizations imply endorsement by the U.S. Government.

536 This work was also partially funded by the Centers of Excellence for Influenza Research and Response
537 (CEIRR, contract # 75N93021C00014, reagent generation), by the Collaborative Influenza Vaccine
538 Innovation Centers (CIVICs contract # 75N93019C00051, reagent generation), P01 AI172531 (PLUTO),
539 U19AI168631 (VIVA) and by institutional funds.

540 This work was supported in part through the computational and data resources and staff expertise
541 provided by Scientific Computing and Data at the Icahn School of Medicine at Mount Sinai and supported
542 by the Clinical and Translational Science Awards (CTSA) grant UL1TR004419 from the National Center for
543 Advancing Translational Sciences. Research reported in this publication was also supported by the Office
544 of Research Infrastructure of the National Institutes of Health under award number S10OD026880 and
545 S10OD030463. The content is solely the responsibility of the authors and does not necessarily represent
546 the official views of the National Institutes of Health.

This work was partially supported by the São Paulo Research Foundation (R.A-S fellowship), projects 2023/02345-7, 2021/05661-1 and 2020/08943-5.

Conflict of interest statement

The Icahn School of Medicine at Mount Sinai has filed patent applications relating to SARS-CoV-2 serological assays, NDV-based SARS-CoV-2 vaccines influenza virus vaccines and influenza virus therapeutics which list Florian Krammer as co-inventor. Dr. Simon is also listed on the SARS-CoV-2 serological assays patent. Mount Sinai has spun out a company, Kantaro, to market serological tests for SARS-CoV-2 and another company, Castlevax, to develop SARS-CoV-2 vaccines. Florian Krammer is co-founder and scientific advisory board member of Castlevax. Florian Krammer has consulted for Merck, Curevac, Seqirus and Pfizer and is currently consulting for 3rd Rock Ventures, GSK, Gritstone and Avimex. The Krammer laboratory is also collaborating with Dynavax on influenza vaccine development. The Ellebedy laboratory has received funding under sponsored research agreements from Moderna, Emergent BioSolutions, and AbbVie. A.H.E. has received consulting and speaking fees from InBios International, Inc, Fimbrion Therapeutics, RGAX, Mubadala Investment Company, AstraZeneca, Moderna, Pfizer, GSK, Danaher, Third Rock Ventures, Goldman Sachs, and Morgan Stanley; is the founder of ImmuneBio Consulting and a recipient of royalties from licensing agreements with Abbvie and Leyden Laboratories B.V.

566 **References**

567 1. The pandemic's true death toll (2023). The Economist. https://www.economist.com/graphic-
568 detail/coronavirus-excess-deaths-estimates.

569 2. Krammer, F. (2023). The role of vaccines in the COVID-19 pandemic: what have we learned? Semin.
570 Immunopathol. 10.1007/s00281-023-00996-2.

571 3. Walls, A.C., Park, Y.-J., Tortorici, M.A., Wall, A., McGuire, A.T., and Veesler, D. (2020). Structure,
572 Function, and Antigenicity of the SARS-CoV-2 Spike Glycoprotein. Cell *181*, 281-292.e6.
573 10.1016/j.cell.2020.02.058.

574 4. Letko, M., Marzi, A., and Munster, V. (2020). Functional assessment of cell entry and receptor usage
575 for SARS-CoV-2 and other lineage B betacoronaviruses. Nat. Microbiol. *5*, 562–569. 10.1038/s41564-
576 020-0688-y.

577 5. Pinto, D., Park, Y.-J., Beltramello, M., Walls, A.C., Tortorici, M.A., Bianchi, S., Jaconi, S., Culap, K.,
578 Zatta, F., De Marco, A., et al. (2020). Cross-neutralization of SARS-CoV-2 by a human monoclonal
579 SARS-CoV antibody. Nature *583*, 290–295. 10.1038/s41586-020-2349-y.

580 6. Tortorici, M.A., Beltramello, M., Lempp, F.A., Pinto, D., Dang, H.V., Rosen, L.E., McCallum, M.,
581 Bowen, J., Minola, A., Jaconi, S., et al. (2020). Ultrapotent human antibodies protect against SARS-
582 CoV-2 challenge via multiple mechanisms. Science *370*, 950–957. 10.1126/science.abe3354.

583 7. McCallum, M., Marco, A.D., Lempp, F.A., Tortorici, M.A., Pinto, D., Walls, A.C., Beltramello, M.,
584 Chen, A., Liu, Z., Zatta, F., et al. (2021). N-terminal domain antigenic mapping reveals a site of
585 vulnerability for SARS-CoV-2. Cell *184*, 2332-2347.e16. 10.1016/j.cell.2021.03.028.

586 8. Tortorici, M.A., Czudnochowski, N., Starr, T.N., Marzi, R., Walls, A.C., Zatta, F., Bowen, J.E., Jaconi, S.,
587 Di Iulio, J., Wang, Z., et al. (2021). Broad sarbecovirus neutralization by a human monoclonal
588 antibody. Nature *597*, 103–108. 10.1038/s41586-021-03817-4.

589 9. Low, J.S., Jerak, J., Tortorici, M.A., McCallum, M., Pinto, D., Cassotta, A., Foglierini, M., Mele, F.,
590 Abdelnabi, R., Weynand, B., et al. (2022). ACE2-binding exposes the SARS-CoV-2 fusion peptide to
591 broadly neutralizing coronavirus antibodies. Science *377*, 735–742. 10.1126/science.abq2679.

592 10. Amanat, F., Thapa, M., Lei, T., Ahmed, S.M.S., Adelsberg, D.C., Carreño, J.M., Strohmeier, S.,
593 Schmitz, A.J., Zafar, S., Zhou, J.Q., et al. (2021). SARS-CoV-2 mRNA vaccination induces functionally
594 diverse antibodies to NTD, RBD, and S2. Cell *184*, 3936-3948.e10. 10.1016/j.cell.2021.06.005.

595 11. Gilbert, P.B., Montefiori, D.C., McDermott, A.B., Fong, Y., Benkeser, D., Deng, W., Zhou, H.,
596 Houchens, C.R., Martins, K., Jayashankar, L., et al. (2022). Immune correlates analysis of the mRNA-
597 1273 COVID-19 vaccine efficacy clinical trial. Science *375*, 43–50. 10.1126/science.abm3425.

598 12. Khoury, D.S., Cromer, D., Reynaldi, A., Schlub, T.E., Wheatley, A.K., Juno, J.A., Subbarao, K., Kent,
599 S.J., Triccas, J.A., and Davenport, M.P. (2021). Neutralizing antibody levels are highly predictive of
600 immune protection from symptomatic SARS-CoV-2 infection. Nat. Med. *27*, 1205–1211.
601 10.1038/s41591-021-01377-8.

602 13. Goldblatt, D., Alter, G., Crotty, Sh., and Plotkin, S. (2022). Correlates of Protection Against SARS CoV-
603 2 Infection and Covid 19 Disease. 10.5281/zenodo.6375936.

604 14. Earle, K.A., Ambrosino, D.M., Fiore-Gartland, A., Goldblatt, D., Gilbert, P.B., Siber, G.R., Dull, P., and
605 Plotkin, S.A. (2021). Evidence for antibody as a protective correlate for COVID-19 vaccines. Vaccine
606 *39*, 4423–4428. 10.1016/j.vaccine.2021.05.063.

607 15. Amanat, F., Thapa, M., Lei, T., Sayed Ahmed, S.M., Adelsberg, D.C., Carreno, J.M., Strohmeier, S.,
608 Schmitz, A.J., Zafar, S., Zhou, J.Q., et al. (2021). The plasmablast response to SARS-CoV-2 mRNA
609 vaccination is dominated by non-neutralizing antibodies and targets both the NTD and the RBD.
610 MedRxiv Prepr. Serv. Health Sci., 2021.03.07.21253098. 10.1101/2021.03.07.21253098.

611 16. Rahman, M.O., Kamigaki, T., Thandar, M.M., Haruyama, R., Yan, F., Shibamura-Fujiogi, M., Khin
612 Maung Soe, J., Islam, M.R., Yoneoka, D., Miyahara, R., et al. (2023). Protection of the third-dose and
613 fourth-dose mRNA vaccines against SARS-CoV-2 Omicron subvariant: a systematic review and meta-
614 analysis. BMJ Open *13*, e076892. 10.1136/bmjopen-2023-076892.

615 17. Vikström, L., Fjällström, P., Gwon, Y.-D., Sheward, D.J., Wigren-Byström, J., Evander, M., Bladh, O.,
616 Widerström, M., Molnar, C., Rasmussen, G., et al. (2023). Vaccine-induced correlate of protection
617 against fatal COVID-19 in older and frail adults during waves of neutralization-resistant variants of
618 concern: an observational study. Lancet Reg. Health – Eur. *30*. 10.1016/j.lanepe.2023.100646.

619 18. Bruhns, P. (2012). Properties of mouse and human IgG receptors and their contribution to disease
620 models. Blood *119*, 5640–5649. 10.1182/blood-2012-01-380121.

621 19. Smyth, M.J., Cretney, E., Kelly, J.M., Westwood, J.A., Street, S.E.A., Yagita, H., Takeda, K., Dommelen,
622 S.L.H. van, Degli-Esposti, M.A., and Hayakawa, Y. (2005). Activation of NK cell cytotoxicity. Mol.
623 Immunol. *42*, 501–510. 10.1016/j.molimm.2004.07.034.

624 20. Tay, M.Z., Wiehe, K., and Pollara, J. (2019). Antibody-Dependent Cellular Phagocytosis in Antiviral
625 Immune Responses. Front. Immunol. *10*, 332. 10.3389/fimmu.2019.00332.

626 21. Hajishengallis, G., Reis, E.S., Mastellos, D.C., Ricklin, D., and Lambris, J.D. (2017). Novel mechanisms
627 and functions of complement. Nat. Immunol. *18*, 1288–1298. 10.1038/ni.3858.

628 22. Vivier, E., Raulet, D.H., Moretta, A., Caligiuri, M.A., Zitvogel, L., Lanier, L.L., Yokoyama, W.M., and
629 Ugolini, S. (2011). Innate or Adaptive Immunity? The Example of Natural Killer Cells. Science *331*,
630 44–49. 10.1126/science.1198687.

631 23. Yeap, W.H., Wong, K.L., Shimasaki, N., Teo, E.C.Y., Quek, J.K.S., Yong, H.X., Diong, C.P., Bertoletti, A.,
632 Linn, Y.C., and Wong, S.C. (2016). CD16 is indispensable for antibody-dependent cellular cytotoxicity
633 by human monocytes. Sci. Rep. *6*, 34310. 10.1038/srep34310.

634 24. Atyeo, C., Fischinger, S., Zohar, T., Slein, M.D., Burke, J., Loos, C., McCulloch, D.J., Newman, K.L.,
635 Wolf, C., Yu, J., et al. (2020). Distinct Early Serological Signatures Track with SARS-CoV-2 Survival.
636 Immunity *53*, 524-532.e4. 10.1016/j.immuni.2020.07.020.

637 25. Bahnan, W., Wrighton, S., Sundwall, M., Bläckberg, A., Larsson, O., Höglund, U., Khakzad, H.,
638 Godzwon, M., Walle, M., Elder, E., et al. (2022). Spike-Dependent Opsonization Indicates Both Dose-

639 Dependent Inhibition of Phagocytosis and That Non-Neutralizing Antibodies Can Confer Protection
640 to SARS-CoV-2. Front. Immunol. *12*.

641 26. Brunet-Ratnasingham, E., Anand, S.P., Gantner, P., Dyachenko, A., Moquin-Beaudry, G., Brassard, N.,
642 Beaudoin-Bussières, G., Pagliuzza, A., Gasser, R., Benlarbi, M., et al. Integrated immunovirological
643 profiling validates plasma SARS-CoV-2 RNA as an early predictor of COVID-19 mortality. Sci. Adv. *7*,
644 eabj5629. 10.1126/sciadv.abj5629.

645 27. Schäfer, A., Muecksch, F., Lorenzi, J.C.C., Leist, S.R., Cipolla, M., Bournazos, S., Schmidt, F., Maison,
646 R.M., Gazumyan, A., Martinez, D.R., et al. (2020). Antibody potency, effector function, and
647 combinations in protection and therapy for SARS-CoV-2 infection in vivoIn vivo efficacy of anti–
648 SARS-CoV-2 antibodies. J. Exp. Med. *218*, e20201993. 10.1084/jem.20201993.

649 28. Winkler, E.S., Gilchuk, P., Yu, J., Bailey, A.L., Chen, R.E., Chong, Z., Zost, S.J., Jang, H., Huang, Y., Allen,
650 J.D., et al. (2021). Human neutralizing antibodies against SARS-CoV-2 require intact Fc effector
651 functions for optimal therapeutic protection. Cell *184*, 1804-1820.e16. 10.1016/j.cell.2021.02.026.

652 29. Zohar, T., Loos, C., Fischinger, S., Atyeo, C., Wang, C., Slein, M.D., Burke, J., Yu, J., Feldman, J.,
653 Hauser, B.M., et al. (2020). Compromised Humoral Functional Evolution Tracks with SARS-CoV-2
654 Mortality. Cell *183*, 1508-1519.e12. 10.1016/j.cell.2020.10.052.

655 30. Altomare, C.G., Adelsberg, D.C., Carreno, J.M., Sapse, I.A., Amanat, F., Ellebedy, A.H., Simon, V.,
656 Krammer, F., and Bajic, G. (2022). Structure of a Vaccine-Induced, Germline-Encoded Human
657 Antibody Defines a Neutralizing Epitope on the SARS-CoV-2 Spike N-Terminal Domain. mBio *13*,
658 e03580-21. 10.1128/mbio.03580-21.

659 31. Leist, S.R., Dinnon, K.H., Schäfer, A., Tse, L.V., Okuda, K., Hou, Y.J., West, A., Edwards, C.E., Sanders,
660 W., Fritch, E.J., et al. (2020). A Mouse-Adapted SARS-CoV-2 Induces Acute Lung Injury and Mortality
661 in Standard Laboratory Mice. Cell *183*, 1070-1085.e12. 10.1016/j.cell.2020.09.050.

662 32. Bianchini, F., Crivelli, V., Abernathy, M.E., Guerra, C., Palus, M., Muri, J., Marcotte, H., Piralla, A.,
663 Pedotti, M., De Gasparo, R., et al. (2023). Human neutralizing antibodies to cold linear epitopes and
664 subdomain 1 of the SARS-CoV-2 spike glycoprotein. Sci. Immunol. *8*, eade0958.
665 10.1126/sciimmunol.ade0958.

666 33. Sun, W., McCroskery, S., Liu, W.-C., Leist, S.R., Liu, Y., Albrecht, R.A., Slamanig, S., Oliva, J., Amanat,
667 F., Schäfer, A., et al. (2020). A Newcastle Disease Virus (NDV) Expressing a Membrane-Anchored
668 Spike as a Cost-Effective Inactivated SARS-CoV-2 Vaccine. Vaccines *8*, 771.
669 10.3390/vaccines8040771.

670 34. Wilkinson, I., Anderson, S., Fry, J., Julien, L.A., Neville, D., Qureshi, O., Watts, G., and Hale, G. (2021).
671 Fc-engineered antibodies with immune effector functions completely abolished. PLoS ONE *16*,
672 e0260954. 10.1371/journal.pone.0260954.

673 35. Saunders, K.O. (2019). Conceptual Approaches to Modulating Antibody Effector Functions and
674 Circulation Half-Life. Front. Immunol. *10*.

675 36. Lustig, Y., Sapir, E., Regev-Yochay, G., Cohen, C., Fluss, R., Olmer, L., Indenbaum, V., Mandelboim,
676 M., Doolman, R., Amit, S., et al. (2021). BNT162b2 COVID-19 vaccine and correlates of humoral

677 immune responses and dynamics: a prospective, single-centre, longitudinal cohort study in health-
678 care workers. Lancet Respir. Med. *9*, 999–1009. 10.1016/S2213-2600(21)00220-4.

679 37. Garcia-Beltran, W.F., Lam, E.C., Astudillo, M.G., Yang, D., Miller, T.E., Feldman, J., Hauser, B.M.,
680 Caradonna, T.M., Clayton, K.L., Nitido, A.D., et al. (2021). COVID-19-neutralizing antibodies predict
681 disease severity and survival. Cell *184*, 476-488.e11. 10.1016/j.cell.2020.12.015.

682 38. Addetia, A., Crawford, K.H.D., Dingens, A., Zhu, H., Roychoudhury, P., Huang, M.-L., Jerome, K.R.,
683 Bloom, J.D., and Greninger, A.L. (2020). Neutralizing Antibodies Correlate with Protection from
684 SARS-CoV-2 in Humans during a Fishery Vessel Outbreak with a High Attack Rate. J. Clin. Microbiol.
685 *58*, 10.1128/jcm.02107-20. 10.1128/jcm.02107-20.

686 39. Nie, J., Li, Q., Wu, J., Zhao, C., Hao, H., Liu, H., Zhang, L., Nie, L., Qin, H., Wang, M., et al. (2020).
687 Quantification of SARS-CoV-2 neutralizing antibody by a pseudotyped virus-based assay. Nat.
688 Protoc. *15*, 3699–3715. 10.1038/s41596-020-0394-5.

689 40. Gunn, B.M., Yu, W.-H., Karim, M.M., Brannan, J.M., Herbert, A.S., Wec, A.Z., Halfmann, P.J., Fusco,
690 M.L., Schendel, S.L., Gangavarapu, K., et al. (2018). A Role for Fc Function in Therapeutic Monoclonal
691 Antibody-Mediated Protection against Ebola Virus. Cell Host Microbe *24*, 221-233.e5.
692 10.1016/j.chom.2018.07.009.

693 41. Dias, A.G., Atyeo, C., Loos, C., Montoya, M., Roy, V., Bos, S., Narvekar, P., Singh, T., Katzelnick, L.C.,
694 Kuan, G., et al. (2022). Antibody Fc characteristics and effector functions correlate with protection
695 from symptomatic dengue virus type 3 infection. Sci. Transl. Med. *14*, eabm3151.
696 10.1126/scitranslmed.abm3151.

697 42. Saphire, E.O., Schendel, S.L., Gunn, B.M., Milligan, J.C., and Alter, G. (2018). Antibody-mediated
698 protection against Ebola virus. Nat. Immunol. *19*, 1169–1178. 10.1038/s41590-018-0233-9.

699 43. Dunand, C.J.H., Leon, P.E., Huang, M., Choi, A., Chromikova, V., Ho, I.Y., Tan, G.S., Cruz, J., Hirsh, A.,
700 Zheng, N.-Y., et al. (2016). Both Neutralizing and Non-Neutralizing Human H7N9 Influenza Vaccine-
701 Induced Monoclonal Antibodies Confer Protection. Cell Host Microbe *19*, 800–813.
702 10.1016/j.chom.2016.05.014.

703 44. Bournazos, S., Klein, F., Pietzsch, J., Seaman, M.S., Nussenzweig, M.C., and Ravetch, J.V. (2014).
704 Broadly Neutralizing Anti-HIV-1 Antibodies Require Fc Effector Functions for In Vivo Activity. Cell
705 *158*, 1243–1253. 10.1016/j.cell.2014.08.023.

706 45. DiLillo, D.J., Palese, P., Wilson, P.C., and Ravetch, J.V. (2016). Broadly neutralizing anti-influenza
707 antibodies require Fc receptor engagement for in vivo protection. J. Clin. Invest. *126*, 605–610.
708 10.1172/JCI84428.

709 46. Vanderven, H.A., Liu, L., Ana-Sosa-Batiz, F., Nguyen, T.H.O., Wan, Y., Wines, B., Hogarth, P.M.,
710 Tilmanis, D., Reynaldi, A., Parsons, M.S., et al. (2017). Fc functional antibodies in humans with
711 severe H7N9 and seasonal influenza. JCI Insight *2*. 10.1172/jci.insight.92750.

712 47. Hessell, A.J., Hangartner, L., Hunter, M., Havenith, C.E.G., Beurskens, F.J., Bakker, J.M., Lanigan,
713 C.M.S., Landucci, G., Forthal, D.N., Parren, P.W.H.I., et al. (2007). Fc receptor but not complement

714 binding is important in antibody protection against HIV. Nature *449*, 101–104.
715 10.1038/nature06106.

716 48. Dreyfus, C., Laursen, N.S., Kwaks, T., Zuijdgeest, D., Khayat, R., Ekiert, D.C., Lee, J.H., Metlagel, Z.,
717 Bujny, M.V., Jongeneelen, M., et al. (2012). Highly Conserved Protective Epitopes on Influenza B
718 Viruses. Science *337*, 1343–1348. 10.1126/science.1222908.

719 49. Sutton, T.C., Lamirande, E.W., Bock, K.W., Moore, I.N., Koudstaal, W., Rehman, M., Weverling, G.J.,
720 Goudsmit, J., and Subbarao, K. (2017). In Vitro Neutralization Is Not Predictive of Prophylactic
721 Efficacy of Broadly Neutralizing Monoclonal Antibodies CR6261 and CR9114 against Lethal H2
722 Influenza Virus Challenge in Mice. J. Virol. *91*, 10.1128/jvi.01603-17. 10.1128/jvi.01603-17.

723 50. Riou, C., Keeton, R., Moyo-Gwete, T., Hermanus, T., Kgagudi, P., Baguma, R., Valley-Omar, Z., Smith,
724 M., Tegally, H., Doolabh, D., et al. (2021). Escape from recognition of SARS-CoV-2 variant spike
725 epitopes but overall preservation of T cell immunity. Sci. Transl. Med. *14*, eabj6824.
726 10.1126/scitranslmed.abj6824.

727 51. Redd, A.D., Nardin, A., Kared, H., Bloch, E.M., Abel, B., Pekosz, A., Laeyendecker, O., Fehlings, M.,
728 Quinn, T.C., and Tobian, A.A.R. (2022). Minimal Crossover between Mutations Associated with
729 Omicron Variant of SARS-CoV-2 and CD8+ T-Cell Epitopes Identified in COVID-19 Convalescent
730 Individuals. mBio *13*, e03617-21. 10.1128/mbio.03617-21.

731 52. Geers, D., Shamier, M.C., Bogers, S., den Hartog, G., Gommers, L., Nieuwkoop, N.N., Schmitz, K.S.,
732 Rijsbergen, L.C., van Osch, J.A.T., Dijkhuizen, E., et al. (2021). SARS-CoV-2 variants of concern
733 partially escape humoral but not T cell responses in COVID-19 convalescent donors and vaccine
734 recipients. Sci. Immunol. *6*, eabj1750. 10.1126/sciimmunol.abj1750.

735 53. Choi, S.J., Kim, D.-U., Noh, J.Y., Kim, S., Park, S.-H., Jeong, H.W., and Shin, E.-C. (2022). T cell epitopes
736 in SARS-CoV-2 proteins are substantially conserved in the Omicron variant. Cell. Mol. Immunol. *19*,
737 447–448. 10.1038/s41423-022-00838-5.

738 54. Keeton, R., Tincho, M.B., Ngomti, A., Baguma, R., Benede, N., Suzuki, A., Khan, K., Cele, S., Bernstein,
739 M., Karim, F., et al. (2022). T cell responses to SARS-CoV-2 spike cross-recognize Omicron. Nature
740 *603*, 488–492. 10.1038/s41586-022-04460-3.

741 55. Ghazizadeh, S., Bolen, J.B., and Fleit, H.B. (1994). Physical and functional association of Src-related
742 protein tyrosine kinases with Fc gamma RII in monocytic THP-1 cells. J. Biol. Chem. *269*, 8878–8884.

743 56. Wang, A.V., Scholl, P.R., and Geha, R.S. (1994). Physical and functional association of the high
744 affinity immunoglobulin G receptor (Fc gamma RI) with the kinases Hck and Lyn. J. Exp. Med. *180*,
745 1165–1170. 10.1084/jem.180.3.1165.

746 57. Odin, J.A., Edberg, J.C., Painter, C.J., Kimberly, R.P., and Unkeless, J.C. (1991). Regulation of
747 Phagocytosis and [Ca2+]i Flux by Distinct Regions of an Fc Receptor. Science *254*, 1785–1788.
748 10.1126/science.1837175.

749 58. Rankin, B.M., Yocum, S.A., Mittler, R.S., and Kiener, P.A. (1993). Stimulation of tyrosine
750 phosphorylation and calcium mobilization by Fc gamma receptor cross-linking. Regulation by the
751 phosphotyrosine phosphatase CD45. J. Immunol. Baltim. Md 1950 *150*, 605–616.

752 59. Ricklin, D., Reis, E.S., and Lambris, J.D. (2016). Complement in disease: a defence system turning
753 offensive. Nat. Rev. Nephrol. *12*, 383–401. 10.1038/nrneph.2016.70.

754 60. Zipfel, P.F., and Skerka, C. (2009). Complement regulators and inhibitory proteins. Nat. Rev.
755 Immunol. *9*, 729–740. 10.1038/nri2620.

756 61. Daha, M.R. (2010). Role of Complement in Innate Immunity and Infections. Crit. Rev. Immunol. *30*.
757 10.1615/CritRevImmunol.v30.i1.30.

758 62. Lund, J., Winter, G., Jones, P.T., Pound, J.D., Tanaka, T., Walker, M.R., Artymiuk, P.J., Arata, Y.,
759 Burton, D.R., and Jefferis, R. (1991). Human Fc gamma RI and Fc gamma RII interact with distinct but
760 overlapping sites on human IgG. J. Immunol. Baltim. Md 1950 *147*, 2657–2662.

761 63. Lo, M., Kim, H.S., Tong, R.K., Bainbridge, T.W., Vernes, J.-M., Zhang, Y., Lin, Y.L., Chung, S., Dennis,
762 M.S., Zuchero, Y.J.Y., et al. (2017). Effector-attenuating Substitutions That Maintain Antibody
763 Stability and Reduce Toxicity in Mice. J. Biol. Chem. *292*, 3900–3908. 10.1074/jbc.M116.767749.

764 64. Ko, S., Park, S., Sohn, M.H., Jo, M., Ko, B.J., Na, J.-H., Yoo, H., Jeong, A.L., Ha, K., Woo, J.R., et al.
765 (2022). An Fc variant with two mutations confers prolonged serum half-life and enhanced effector
766 functions on IgG antibodies. Exp. Mol. Med. *54*, 1850–1861. 10.1038/s12276-022-00870-5.

767 65. Mangeat, T., Gracia, M., Pichard, A., Poty, S., Martineau, P., Robert, B., and Deshayes, E. (2023). Fc-
768 engineered monoclonal antibodies to reduce off-target liver uptake. EJNMMI Res. *13*, 81.
769 10.1186/s13550-023-01030-0.

770 66. Mausser, E., Nador, E., Politch, J.A., Pauly, M.R., Marathe, J.G., Moench, T.R., Zeitlin, L., Whaley, K.J.,
771 and Anderson, D.J. (2023). LALAPG variant of the Human Contraception Antibody (HCA) reduces Fc-
772 mediated effector functions while maintaining sperm agglutination activity. PLOS ONE *18*,
773 e0282147. 10.1371/journal.pone.0282147.

774 67. Bournazos, S., DiLillo, D.J., Goff, A.J., Glass, P.J., and Ravetch, J.V. (2019). Differential requirements
775 for FcγR engagement by protective antibodies against Ebola virus. Proc. Natl. Acad. Sci. *116*, 20054–
776 20062. 10.1073/pnas.1911842116.

777 68. Yuan, Y., Cao, D., Zhang, Y., Ma, J., Qi, J., Wang, Q., Lu, G., Wu, Y., Yan, J., Shi, Y., et al. (2017). Cryo-
778 EM structures of MERS-CoV and SARS-CoV spike glycoproteins reveal the dynamic receptor binding
779 domains. Nat. Commun. *8*, 15092. 10.1038/ncomms15092.

780 69. Singh, G., Abbad, A., Kleiner, G., Srivastava, K., Gleason, C., PARIS Study Group, Carreño, J.M., Simon,
781 V., and Krammer, F. (2023). The post-COVID-19 population has a high prevalence of cross-reactive
782 antibodies to spikes from all Orthocoronavirinae genera. mBio *15*, e02250-23. 10.1128/mbio.02250-
783 23.

784 70. Shimizu, J., Sasaki, T., Koketsu, R., Morita, R., Yoshimura, Y., Murakami, A., Saito, Y., Kusunoki, T.,
785 Samune, Y., Nakayama, E.E., et al. (2022). Reevaluation of antibody-dependent enhancement of
786 infection in anti-SARS-CoV-2 therapeutic antibodies and mRNA-vaccine antisera using FcR- and
787 ACE2-positive cells. Sci. Rep. *12*, 15612. 10.1038/s41598-022-19993-w.

788 71. Wang, S., Peng, Y., Wang, R., Jiao, S., Wang, M., Huang, W., Shan, C., Jiang, W., Li, Z., Gu, C., et al.
789 (2020). Characterization of neutralizing antibody with prophylactic and therapeutic efficacy against
790 SARS-CoV-2 in rhesus monkeys. Nat. Commun. *11*, 5752. 10.1038/s41467-020-19568-1.

791 72. Li, D., Edwards, R.J., Manne, K., Martinez, D.R., Schäfer, A., Alam, S.M., Wiehe, K., Lu, X., Parks, R.,
792 Sutherland, L.L., et al. (2021). *In vitro* and *in vivo* functions of SARS-CoV-2 infection-enhancing and
793 neutralizing antibodies. Cell *184*, 4203-4219.e32. 10.1016/j.cell.2021.06.021.

794 73. Liu, Y., Soh, W.T., Kishikawa, J., Hirose, M., Nakayama, E.E., Li, S., Sasai, M., Suzuki, T., Tada, A.,
795 Arakawa, A., et al. (2021). An infectivity-enhancing site on the SARS-CoV-2 spike protein targeted by
796 antibodies. Cell *184*, 3452-3466.e18. 10.1016/j.cell.2021.05.032.

797 74. Dekkers, G., Bentlage, A.E.H., Stegmann, T.C., Howie, H.L., Lissenberg-Thunnissen, S., Zimring, J.,
798 Rispens, T., and Vidarsson, G. (2017). Affinity of human IgG subclasses to mouse Fc gamma
799 receptors. mAbs *9*, 767–773. 10.1080/19420862.2017.1323159.

800 75. Yamin, R., Jones, A.T., Hoffmann, H.-H., Schäfer, A., Kao, K.S., Francis, R.L., Sheahan, T.P., Baric, R.S.,
801 Rice, C.M., Ravetch, J.V., et al. (2021). Fc-engineered antibody therapeutics with improved anti-
802 SARS-CoV-2 efficacy. Nature *599*, 465–470. 10.1038/s41586-021-04017-w.

803 76. Rogers, K.A., Scinicariello, F., and Attanasio, R. (2006). IgG Fc receptor III homologues in nonhuman
804 primate species: genetic characterization and ligand interactions. J. Immunol. Baltim. Md 1950 *177*,
805 3848–3856. 10.4049/jimmunol.177.6.3848.

806 77. Smith, P., DiLillo, D.J., Bournazos, S., Li, F., and Ravetch, J.V. (2012). Mouse model recapitulating
807 human Fcγ receptor structural and functional diversity. Proc. Natl. Acad. Sci. U. S. A. *109*, 6181–
808 6186. 10.1073/pnas.1203954109.

809 78. Carreño, J.M., Singh, G., Simon, V., and Krammer, F. (2023). Bivalent COVID-19 booster vaccines and
810 the absence of BA.5-specific antibodies. Lancet Microbe *4*, e569. 10.1016/S2666-5247(23)00118-0.

811 79. Stadlbauer, D., Amanat, F., Chromikova, V., Jiang, K., Strohmeier, S., Arunkumar, G.A., Tan, J.,
812 Bhavsar, D., Capuano, C., Kirkpatrick, E., et al. (2020). SARS-CoV-2 Seroconversion in Humans: A
813 Detailed Protocol for a Serological Assay, Antigen Production, and Test Setup. Curr. Protoc.
814 Microbiol. *57*, e100. 10.1002/cpmc.100.

815 80. Amanat, F., Stadlbauer, D., Strohmeier, S., Nguyen, T.H.O., Chromikova, V., McMahon, M., Jiang, K.,
816 Arunkumar, G.A., Jurczyszak, D., Polanco, J., et al. (2020). A serological assay to detect SARS-CoV-2
817 seroconversion in humans. Nat. Med. *26*, 1033–1036. 10.1038/s41591-020-0913-5.

818 81. Carreño, J.M., Alshammary, H., Tcheou, J., Singh, G., Raskin, A.J., Kawabata, H., Sominsky, L.A., Clark,
819 J.J., Adelsberg, D.C., Bielak, D.A., et al. (2022). Activity of convalescent and vaccine serum against
820 SARS-CoV-2 Omicron. Nature *602*, 682–688. 10.1038/s41586-022-04399-5.

821 82. Lara-Puente, J.H., Carreño, J.M., Sun, W., Suárez-Martínez, A., Ramírez-Martínez, L., Quezada-
822 Monroy, F., Paz-De la Rosa, G., Vigueras-Moreno, R., Singh, G., Rojas-Martínez, O., et al. Safety and
823 Immunogenicity of a Newcastle Disease Virus Vector-Based SARS-CoV-2 Vaccine Candidate,
824 AVX/COVID-12-HEXAPRO (Patria), in Pigs. mBio *12*, e01908-21. 10.1128/mBio.01908-21.

825 83. Hsieh, C.-L., Goldsmith, J.A., Schaub, J.M., DiVenere, A.M., Kuo, H.-C., Javanmardi, K., Le, K.C.,
826 Wrapp, D., Lee, A.G., Liu, Y., et al. (2020). Structure-based design of prefusion-stabilized SARS-CoV-2
827 spikes. Science *369*, 1501–1505. 10.1126/science.abd0826.

828 84. Zheng, S.Q., Palovcak, E., Armache, J.-P., Verba, K.A., Cheng, Y., and Agard, D.A. (2017). MotionCor2:
829 anisotropic correction of beam-induced motion for improved cryo-electron microscopy. Nat.
830 Methods *14*, 331–332. 10.1038/nmeth.4193.

831 85. Punjani, A., Rubinstein, J.L., Fleet, D.J., and Brubaker, M.A. (2017). cryoSPARC: algorithms for rapid
832 unsupervised cryo-EM structure determination. Nat. Methods *14*, 290–296. 10.1038/nmeth.4169.

833 86. Dunbar, J., Krawczyk, K., Leem, J., Marks, C., Nowak, J., Regep, C., Georges, G., Kelm, S., Popovic, B.,
834 and Deane, C.M. (2016). SAbPred: a structure-based antibody prediction server. Nucleic Acids Res.
835 *44*, W474-478. 10.1093/nar/gkw361.

836 87. Meng, E.C., Goddard, T.D., Pettersen, E.F., Couch, G.S., Pearson, Z.J., Morris, J.H., and Ferrin, T.E.
837 (2023). UCSF ChimeraX: Tools for structure building and analysis. Protein Sci. Publ. Protein Soc. *32*,
838 e4792. 10.1002/pro.4792.

839 88. Emsley, P., Lohkamp, B., Scott, W.G., and Cowtan, K. (2010). Features and development of Coot.
840 Acta Crystallogr. D Biol. Crystallogr. *66*, 486–501. 10.1107/S0907444910007493.

841 89. Agirre, J., Iglesias-Fernández, J., Rovira, C., Davies, G.J., Wilson, K.S., and Cowtan, K.D. (2015).
842 Privateer: software for the conformational validation of carbohydrate structures. Nat. Struct. Mol.
843 Biol. *22*, 833–834. 10.1038/nsmb.3115.

844 90. Liebschner, D., Afonine, P.V., Baker, M.L., Bunkóczi, G., Chen, V.B., Croll, T.I., Hintze, B., Hung, L.W.,
845 Jain, S., McCoy, A.J., et al. (2019). Macromolecular structure determination using X-rays, neutrons
846 and electrons: recent developments in Phenix. Acta Crystallogr. Sect. Struct. Biol. *75*, 861–877.
847 10.1107/S2059798319011471.

848 91. Williams, C.J., Headd, J.J., Moriarty, N.W., Prisant, M.G., Videau, L.L., Deis, L.N., Verma, V., Keedy,
849 D.A., Hintze, B.J., Chen, V.B., et al. (2018). MolProbity: More and better reference data for improved
850 all-atom structure validation. Protein Sci. Publ. Protein Soc. *27*, 293–315. 10.1002/pro.3330.

851 92. Morin, A., Eisenbraun, B., Key, J., Sanschagrin, P.C., Timony, M.A., Ottaviano, M., and Sliz, P. (2013).
852 Collaboration gets the most out of software. eLife *2*, e01456. 10.7554/eLife.01456.

853 **Figure legends**

854 **Figure 1. Characterization of mAb binding and neutralization against SARS-CoV-2 variants. (A-D)** Binding
855 of RBD-specific **(A)**, NTD-specific **(B)**, S2-specific **(C)**, and unknown epitope-specific **(D)** SARS-CoV-2 mAbs
856 to the spike proteins of SARS-CoV-2 variants. Neutralizing mAbs are denoted with red Ns. **(E)** Neutralizing
857 activity of the neutralizing mAbs against authentic SARS-CoV-2 variants.

858 **Figure 2. Investigating the protection elicited by the mAbs using lethal animal challenge models. (A-D)**
859 Maximum weight loss and survival of BALB/cAnNHsd mice treated with RBD-specific **(A)**, NTD-specific **(B)**,

860 S2-specific **(C)**, and unknown epitope-specific **(D)** SARS-CoV-2 mAbs prior to lethal challenge with mouse-
861 adapted SARS-CoV-2. **(E)** Hamster weight loss following treatment with the 6 most protective mAbs and
862 challenge with wild type SARS-CoV-2. Neutralizing mAbs are shown as crosses, while non-neutralizing
863 mAbs are shown as circles. In **(A-D)**, the vertical bars in the maximum weight loss graphs indicates the
864 mean with standard deviation. P values are shown only for statistically significant comparisons as
865 determined by a Kruskal-Wallis with Dunn's multiple comparisons test.

866 **Figure 3. Mouse lung titers following mAb treatment and SARS-CoV-2 challenge. (A-D)** murine lung titers
867 3 dpi after treatment with RBD-specific **(A)**, NTD-specific **(B)**, S2-specific **(C)**, and unknown epitope-specific
868 **(D)** SARS-CoV-2 mAbs and challenge with mouse adapted SARS-CoV-2. **(E-H)** lung titers 5 dpi after
869 treatment with RBD-specific **(E)**, NTD-specific **(F)**, S2-specific **(G)**, and unknown epitope-specific **(H)** SARS-
870 CoV-2 mAbs and challenge with mouse adapted SARS-CoV-2. Neutralizing mAbs are shown as crosses,
871 while non-neutralizing mAbs are shown as circles. P values are shown only for groups with titers
872 statistically significant compared to the negative control, as determined by an ordinary one-way ANOVA
873 with Dunnett's multiple comparisons test with a single pooled variance.

874 **Figure 4. Cryo-EM structures of PVI.V6-12, PVI.V3-21, and PVI.V5-4 in complex with SARS-CoV-2 spike.**
875 (**A**) and (**B**) Global, modest-resolution cryo-EM maps of PVI.V6-12 and PVI.V3-21 Fabs in complex with
876 spike. The structures identify the binding epitopes on the spike RBD. Fabs are colored green, RBD sienna,
877 and the rest of spike blue. (**C**) Cryo-EM map of PVI.V5-4 in complex with spike at 3.67Å nominal resolution.
878 The structure defines the PVI.V5-4 epitope on the sub-domain 1 (SD1). Spike S1 including RBD, SD1, and
879 SD2 domains are colored sienna, S2 dark grey, and PVI.5-4 variable heavy and light chains blue and green,
880 respectively. (**D**) Cartoon representation of the atomic model of PVI.V5-4 in complex with spike SD1. Major
881 interactions are defined by the antibody HCDR3, HCDR2, and LCDR3 loops. N318 glycan is shown for
882 context. € Surface representation of PVI.V5-4 epitope on spike SD1. The Fab interacting loops are shown
883 as cartoon, and individual interacting residues are labeled and shown as sticks. The spike interacting
884 residues are underlined. N318 glycan is shown for context.

885 **Figure 5. Characterization of the Fc-mediated activity of the mAbs. (A)** FcγRIIIa reporter activity of the
886 RBD, NTD, S2, and unknown epitope binding mAbs. **(B)** FcγRIIa reporter activity of the RBD, NTD, S2, and
887 unknown epitope binding mAbs. **(C)** Binding of complement protein C1q to the Fc portion of the mAbs in
888 the presence of wild type SARS-CoV-2 spike protein. Dotted lines denote the limit of detection.

889 **Figure 6. Investigating the protection elicited by Fc-silent mutant mAbs. (A)** FcγRIIIa reporter activity of
890 the seven most protective mAbs and their LALA and LALAPG mutant counterparts. **(B)** FcγRIIa reporter
891 activity of the wild type, LALA, and LALAPG mAbs. **(C)** Binding of complement protein C1q by the wild type,
892 LALA, and LALAPG mAbs in the presence of wild type SARS-CoV-2 spike protein. Dotted lines denote the
893 limit of detection. **(D)** Weight loss and survival of BALB/cAnNHsd mice treated the seven most protective
894 mAbs and their LALA and LALAPG counterparts following lethal challenge with mouse-adapted SARS-CoV-
895 2.

896 **Figure S1. Neutralizing activity of the mAbs at high concentration.** Neutralizing activity of the mAbs
897 against authentic SARS-CoV-2 at a starting concentration of 200 µg/ml. Only mAbs exhibiting detectable
898 neutralization are shown.

899 **Figure S2. Protection elicited by the 7 most protective mAbs in the K18 murine model. (A)** Weight loss
900 and survival in transgenic K18 mice following treatment with mAbs and challenge with a 3x LD_{50} dose of
901 wild type SARS-CoV-2. **(B)** Weight loss and survival in K18 mice following treatment with mAbs and
902 challenge with a 5x LD_{50} dose of wild type SARS-CoV-2.

903 **Figure S3. Binding of wild type, LALA, and LALAPG mAbs to SARS-CoV-2 spike.** Binding of the seven most
904 protective SARS-CoV-2 mAbs and their mutant LALA and LALAPG equivalents to wild type SARS-CoV-2
905 spike.

906 **Figure S4. Cryo-EM data processing scheme and local resolution estimation of the final map.**

907 (**A**) Representative electron micrograph and (**B**) 2D class averages obtained for the SARS-CoV-2 Spike
908 ectodomain in complex with PVI.V5-4 Fab. (**C**) Local resolution and (**D**) gold-standard Fourier shell
909 correlation curves calculated with cryoSPARC v3.3.1. for the locally refined S1-Fab complex. Detailed cryo-
910 EM data processing workflow for the global (**E**) and local (**F**) maps. See the Methods section for more
911 details.

912

913

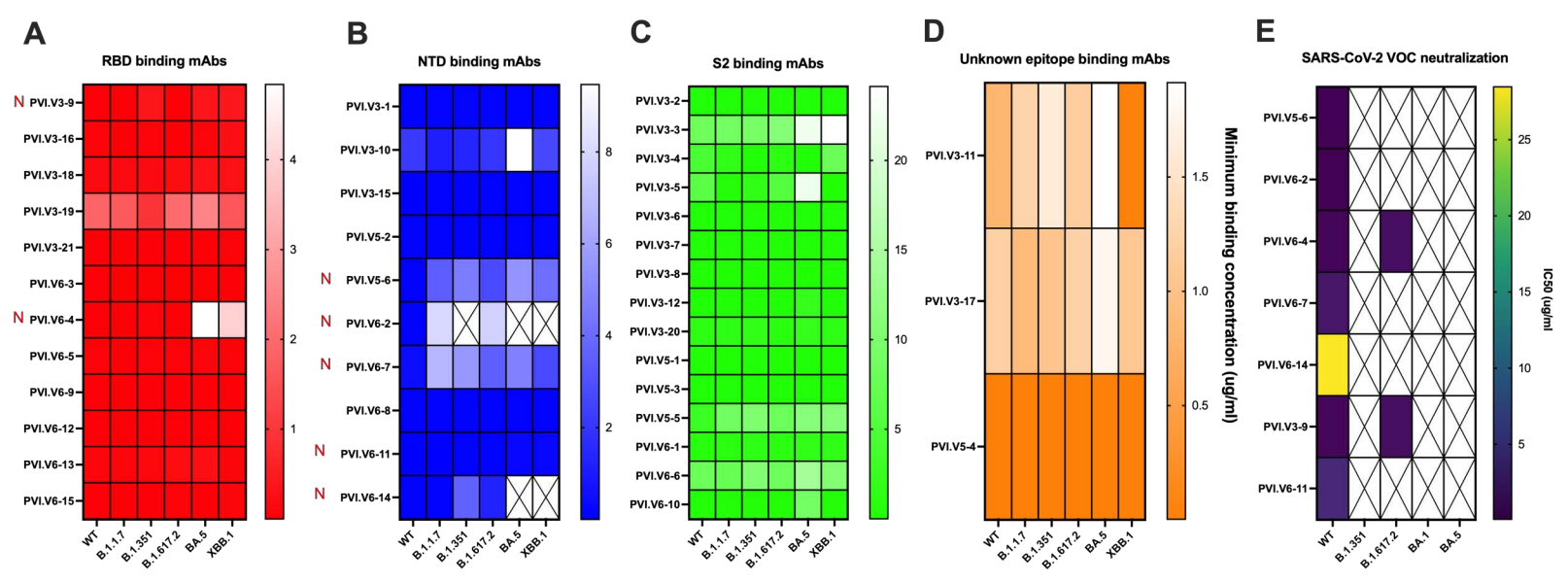
A
RBD binding mAbs
N PVI.V3-9
PVI.V3-16
PVI.V3-18
PVI.V3-19
PVI.V3-21
PVI.V6-3
N PVI.V6-4
PVI.V6-5
PVI.V6-9
PVI.V6-12
PVI.V6-13
PVI.V6-15
WT
B.1.1.7
B.1.351
B.1.617.2
BA.5
XBB.1
4
3
2
1
B
NTD binding mAbs
PVI.V3-1
PVI.V3-10
PVI.V3-15
PVI.V5-2
N PVI.V5-6
N PVI.V6-2
N PVI.V6-7
PVI.V6-8
N PVI.V6-11
N PVI.V6-14
WT
B.1.1.7
B.1.351
B.1.617.2
BA.5
XBB.1
8
6
4
2
C
S2 binding mAbs
PVI.V3-2
PVI.V3-3
PVI.V3-4
PVI.V3-5
PVI.V3-6
PVI.V3-7
PVI.V3-8
PVI.V3-12
PVI.V3-20
PVI.V5-1
PVI.V5-3
PVI.V5-5
PVI.V6-1
PVI.V6-6
PVI.V6-10
WT
B.1.1.7
B.1.351
B.1.617.2
BA.5
XBB.1
20
15
10
5
D
Unknown epitope binding mAbs
PVI.V3-11
PVI.V3-17
PVI.V5-4
WT
B.1.1.7
B.1.351
B.1.617.2
BA.5
XBB.1
1.5
1.0
0.5
Minimum binding concentration (ug/ml)
E
SARS-CoV-2 VOC neutralization
PVI.V5-6
PVI.V6-2
PVI.V6-4
PVI.V6-7
PVI.V6-14
PVI.V3-9
PVI.V6-11
WT
B.1.351
B.1.617.2
BA.1
BA.5
25
20
15
10
5
IC50 (ug/ml

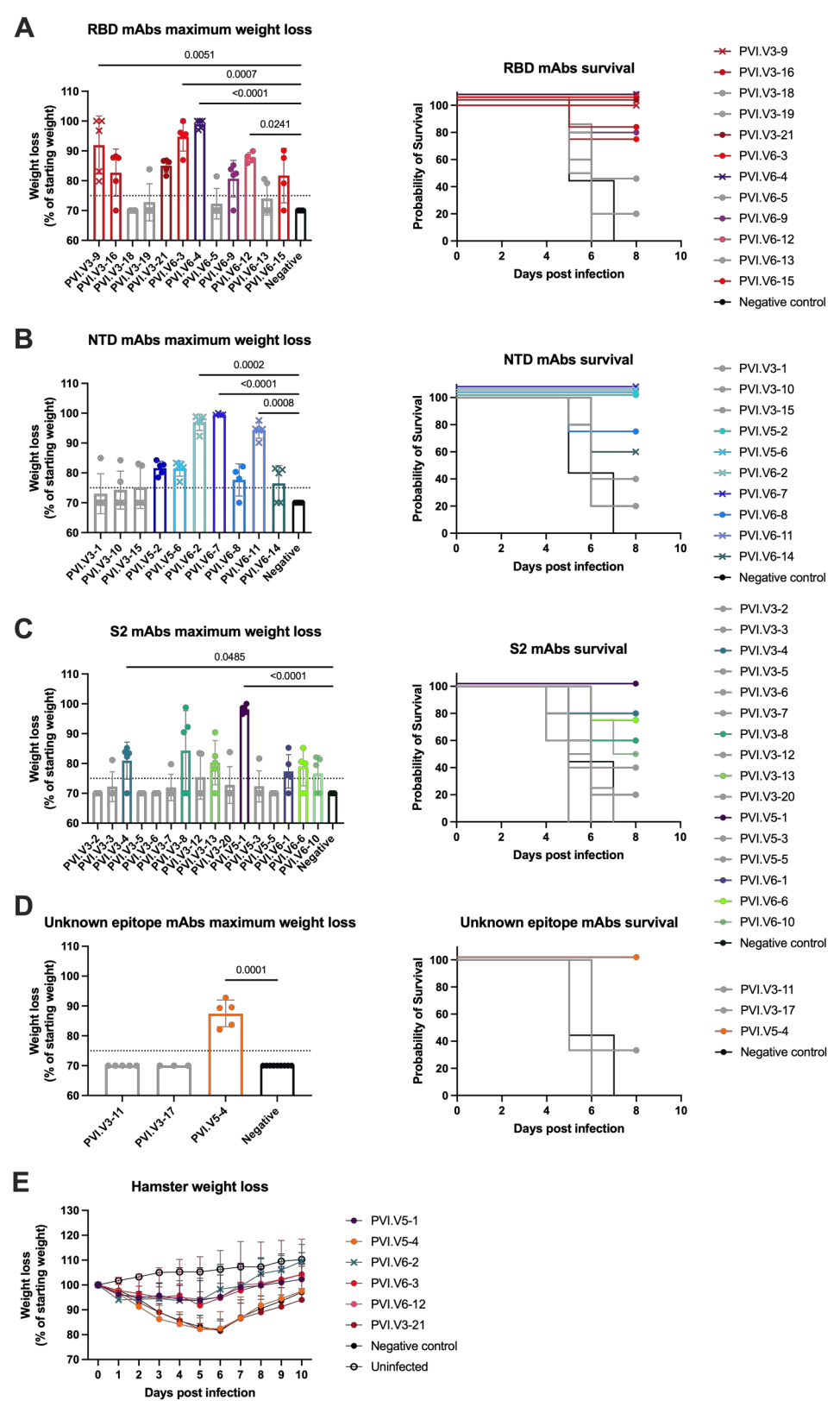
A
RBD mAbs maximum weight loss
0.0051
0.0007
<0.0001
0.0241
Weight loss (% of starting weight)
PVI.V3-9
PVI.V3-16
PVI.V3-18
PVI.V3-19
PVI.V3-21
PVI.V6-3
PVI.V6-4
PVI.V6-5
PVI.V6-9
PVI.V6-12
PVI.V6-13
PVI.V6-15
Negative
RBD mAbs survival
Probability of Survival
Days post infection
PVI.V3-9
PVI.V3-16
PVI.V3-18
PVI.V3-19
PVI.V3-21
PVI.V6-3
PVI.V6-4
PVI.V6-5
PVI.V6-9
PVI.V6-12
PVI.V6-13
PVI.V6-15
Negative control
B
NTD mAbs maximum weight loss
0.0002
<0.0001
0.0008
Weight loss (% of starting weight)
PVI.V3-1
PVI.V3-10
PVI.V3-15
PVI.V5-2
PVI.V5-6
PVI.V6-2
PVI.V6-7
PVI.V6-8
PVI.V6-11
PVI.V6-14
Negative
NTD mAbs survival
Probability of Survival
Days post infection
PVI.V3-1
PVI.V3-10
PVI.V3-15
PVI.V5-2
PVI.V5-6
PVI.V6-2
PVI.V6-7
PVI.V6-8
PVI.V6-11
PVI.V6-14
Negative control
C
S2 mAbs maximum weight loss
0.0485
<0.0001
Weight loss (% of starting weight)
PVI.V3-2
PVI.V3-3
PVI.V3-4
PVI.V3-5
PVI.V3-6
PVI.V3-7
PVI.V3-8
PVI.V3-12
PVI.V3-13
PVI.V3-20
PVI.V5-1
PVI.V5-3
PVI.V5-5
PVI.V6-1
PVI.V6-6
PVI.V6-10
Negative
S2 mAbs survival
Probability of Survival
Days post infection
PVI.V3-2
PVI.V3-3
PVI.V3-4
PVI.V3-5
PVI.V3-6
PVI.V3-7
PVI.V3-8
PVI.V3-12
PVI.V3-13
PVI.V3-20
PVI.V5-1
PVI.V5-3
PVI.V5-5
PVI.V6-1
PVI.V6-6
PVI.V6-10
Negative control
D
Unknown epitope mAbs maximum weight loss
0.0001
Weight loss (% of starting weight)
PVI.V3-11
PVI.V3-17
PVI.V5-4
Negative
Unknown epitope mAbs survival
Probability of Survival
Days post infection
PVI.V3-11
PVI.V3-17
PVI.V5-4
Negative control
E
Hamster weight loss
Weight loss (% of starting weight)
Days post infection
PVI.V5-1
PVI.V5-4
PVI.V6-2
PVI.V6-3
PVI.V6-12
PVI.V3-21
Negative control
Uninfected

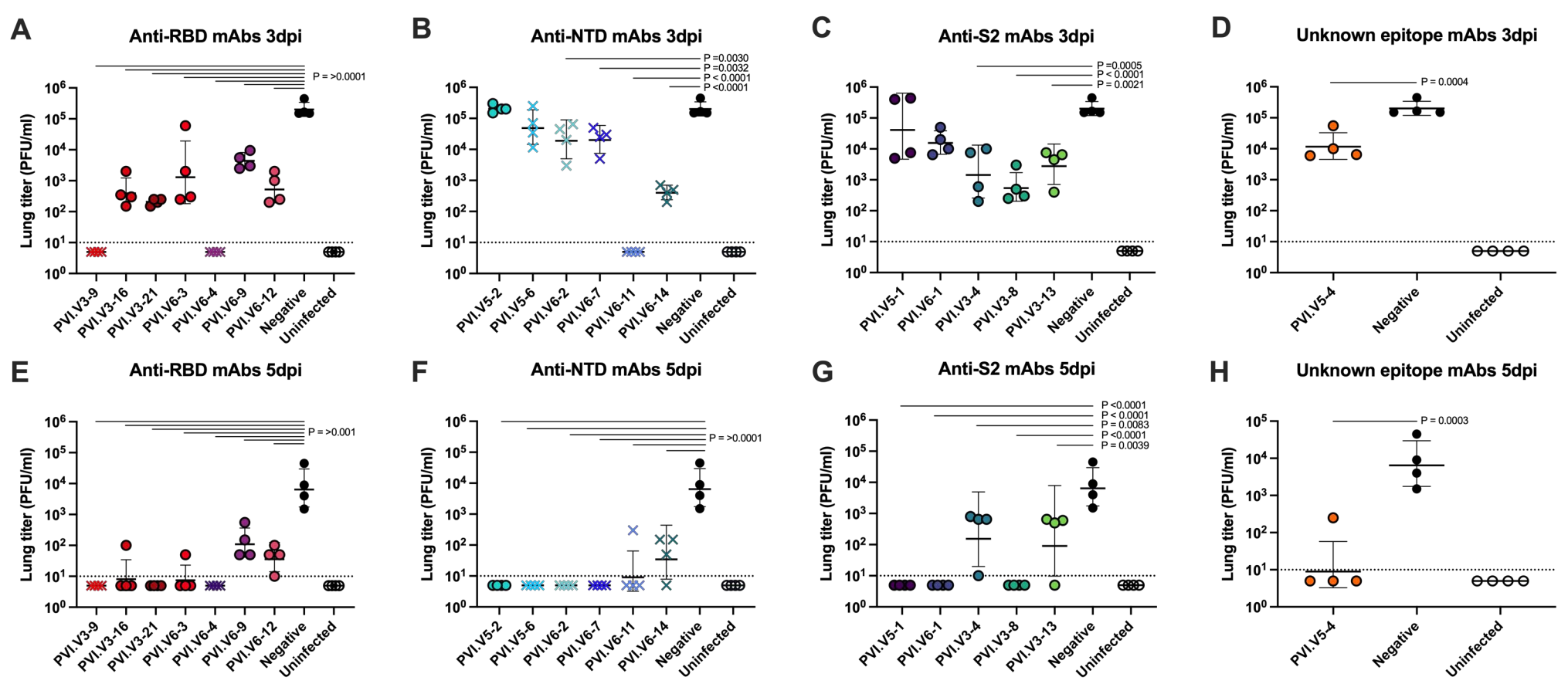
A
Anti-RBD mAbs 3dpi
P = >0.0001
Lung titer (PFU/ml)
PVI.V3-9
PVI.V3-16
PVI.V3-21
PVI.V6-3
PVI.V6-4
PVI.V6-9
PVI.V6-12
Negative
Uninfected
B
Anti-NTD mAbs 3dpi
P =0.0030
P =0.0032
P < 0.0001
P <0.0001
Lung titer (PFU/ml)
PVI.V5-2
PVI.V5-6
PVI.V6-2
PVI.V6-7
PVI.V6-11
PVI.V6-14
Negative
Uninfected
C
Anti-S2 mAbs 3dpi
P =0.0005
P < 0.0001
P = 0.0021
Lung titer (PFU/ml)
PVI.V5-1
PVI.V6-1
PVI.V3-4
PVI.V3-8
PVI.V3-13
Negative
Uninfected
D
Unknown epitope mAbs 3dpi
P = 0.0004
Lung titer (PFU/ml)
PVI.V5-4
Negative
Uninfected
E
Anti-RBD mAbs 5dpi
P = >0.001
Lung titer (PFU/ml)
PVI.V3-9
PVI.V3-16
PVI.V3-21
PVI.V6-3
PVI.V6-4
PVI.V6-9
PVI.V6-12
Negative
Uninfected
F
Anti-NTD mAbs 5dpi
P = >0.0001
Lung titer (PFU/ml)
PVI.V5-2
PVI.V5-6
PVI.V6-2
PVI.V6-7
PVI.V6-11
PVI.V6-14
Negative
Uninfected
G
Anti-S2 mAbs 5dpi
P <0.0001
P < 0.0001
P = 0.0083
P <0.0001
P = 0.0039
Lung titer (PFU/ml)
PVI.V5-1
PVI.V6-1
PVI.V3-4
PVI.V3-8
PVI.V3-13
Negative
Uninfected
H
Unknown epitope mAbs 5dpi
P = 0.0003
Lung titer (PFU/ml)
PVI.V5-4
Negative
Uninfected

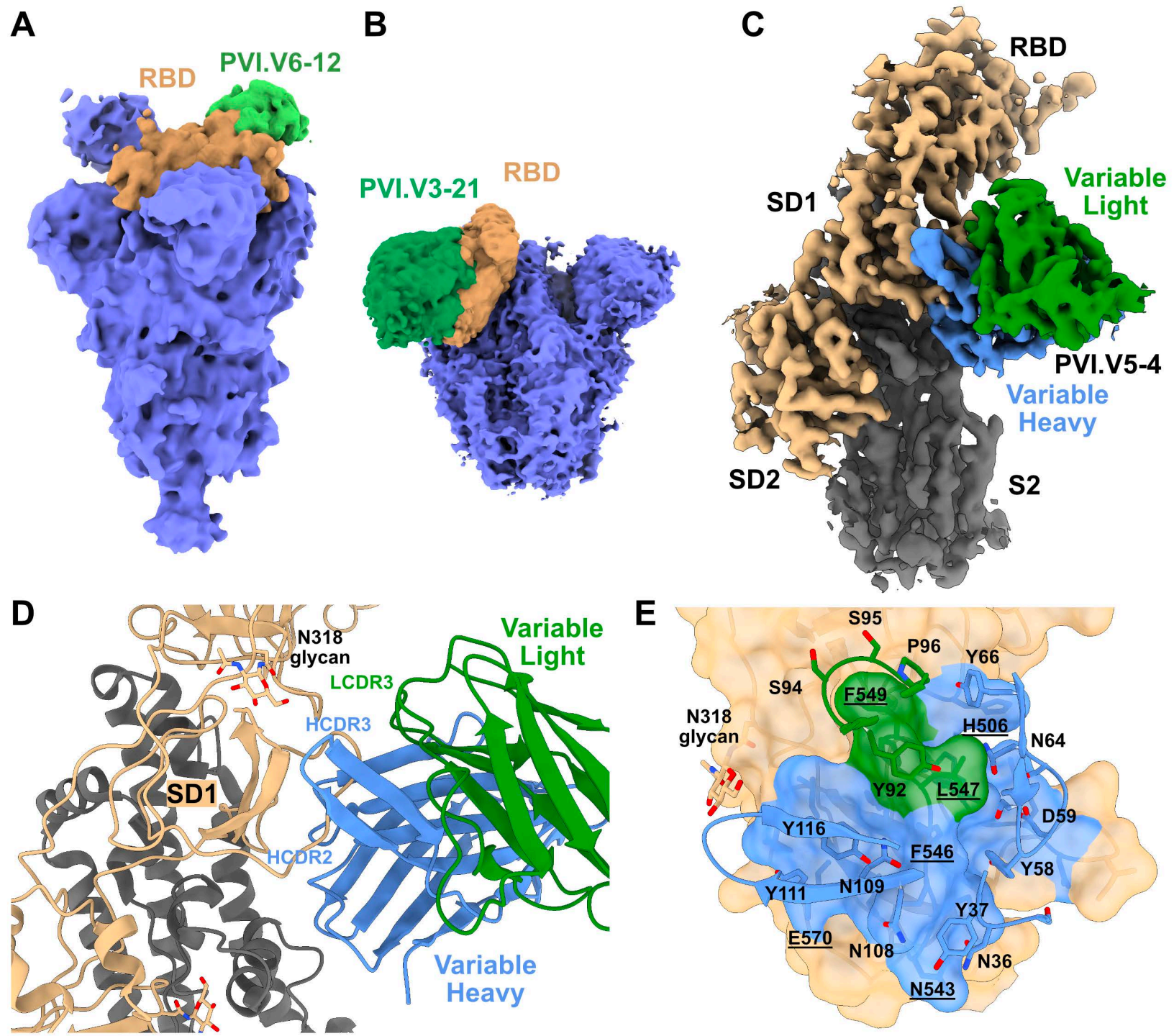
A
RBD
PVI.V6-12
B
PVI.V3-21
RBD
C
RBD
SD1
Variable
Light
PVI.V5-4
Variable
Heavy
SD2
S2
D
N318
glycan
LCDR3
Variable
Light
HCDR3
SD1
HCDR2
Variable
Heavy
E
S95
P96
Y66
S94
F549
N318
glycan
H506
N64
Y92
L547
D59
Y116
F546
Y58
Y111
N109
Y37
E570
N108
N36
N543

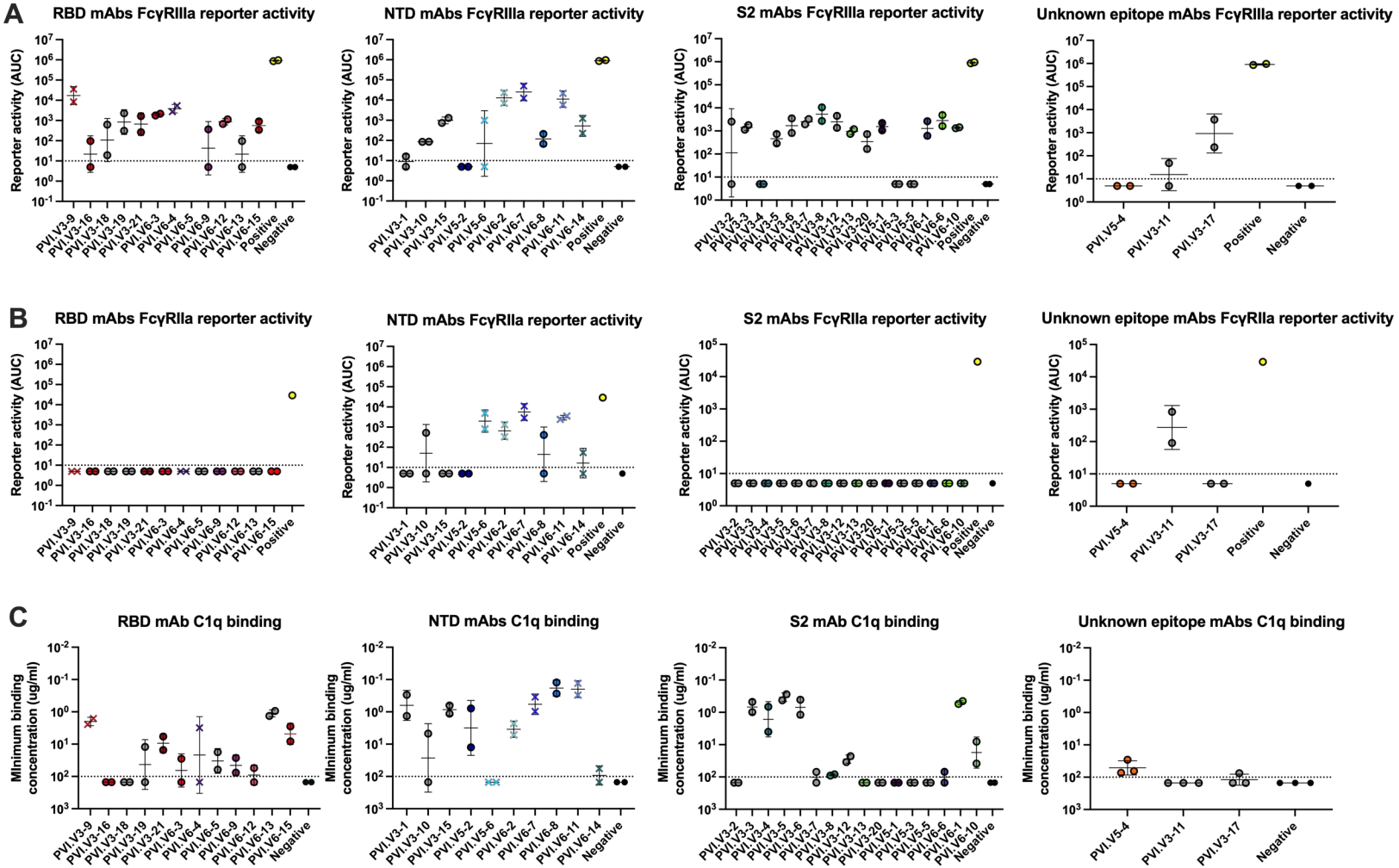
A
RBD mAbs FcγRIIIa reporter activity
NTD mAbs FcγRIIIa reporter activity
S2 mAbs FcγRIIIa reporter activity
Unknown epitope mAbs FcγRIIIa reporter activity
Reporter activity (AUC)
PVI.V3-9
PVI.V3-16
PVI.V3-18
PVI.V3-19
PVI.V3-21
PVI.V6-3
PVI.V6-4
PVI.V6-5
PVI.V6-9
PVI.V6-12
PVI.V6-13
PVI.V6-15
Positive
Negative
PVI.V3-1
PVI.V3-10
PVI.V3-15
PVI.V5-2
PVI.V5-6
PVI.V6-2
PVI.V6-7
PVI.V6-8
PVI.V6-11
PVI.V6-14
PVI.V3-2
PVI.V3-3
PVI.V3-4
PVI.V3-5
PVI.V3-6
PVI.V3-7
PVI.V3-8
PVI.V3-12
PVI.V3-13
PVI.V3-20
PVI.V5-1
PVI.V5-3
PVI.V5-5
PVI.V6-1
PVI.V6-6
PVI.V6-10
PVI.V5-4
PVI.V3-11
PVI.V3-17
B
RBD mAbs FcγRIIa reporter activity
NTD mAbs FcγRIIa reporter activity
S2 mAbs FcγRIIa reporter activity
Unknown epitope mAbs FcγRIIa reporter activity
C
RBD mAb C1q binding
NTD mAbs C1q binding
S2 mAb C1q binding
Unknown epitope mAbs C1q binding
MInimum binding concentration (ug/ml)

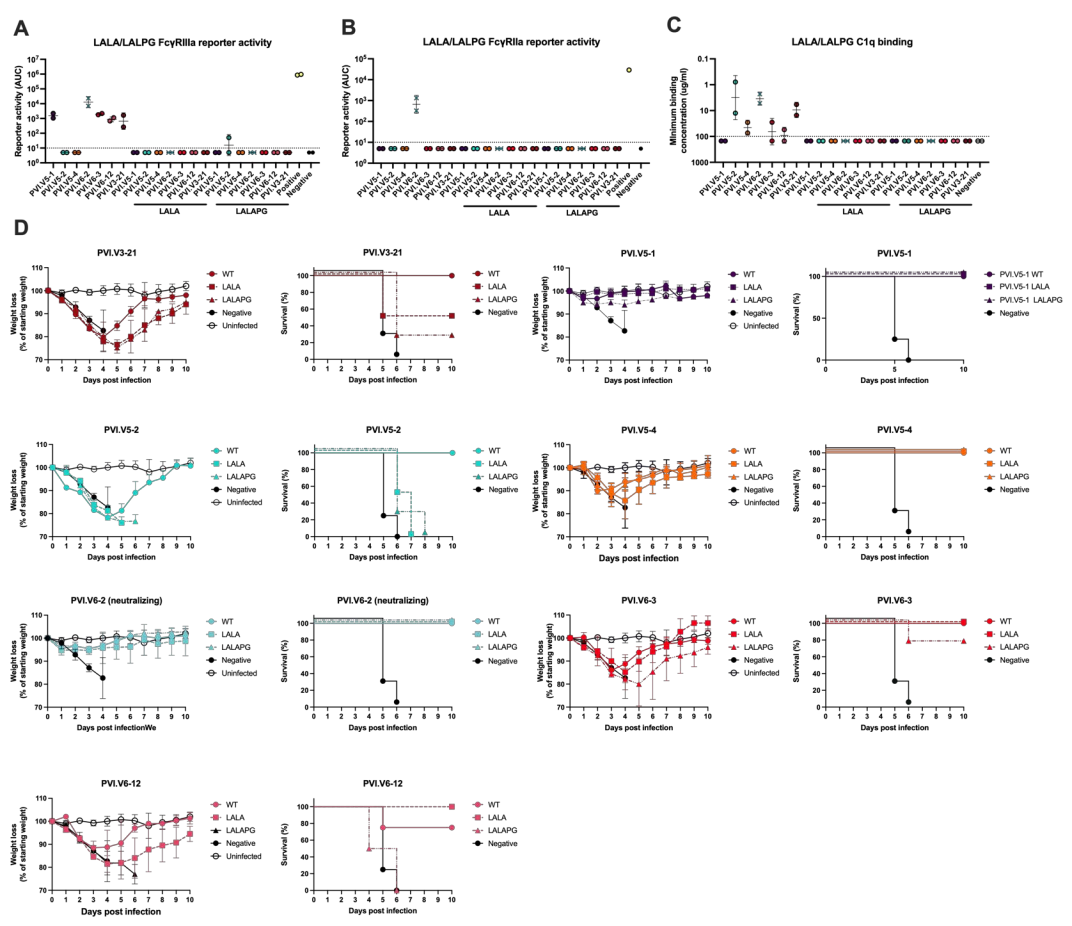
A
LALA/LALPG FcγRIIIa reporter activity
Reporter activity (AUC)
B
LALA/LALPG FcγRIIa reporter activity
Reporter activity (AUC)
C
LALA/LALPG C1q binding
Minimum binding concentration (ng/ml)
PVI.V5-1
PVI.V5-2
PVI.V5-4
PVI.V6-2
PVI.V6-3
PVI.V6-12
PVI.V3-21
Positive
Negative
LALA
LALAPG
D
PVI.V3-21
PVI.V5-1
PVI.V5-2
PVI.V5-4
PVI.V6-2 (neutralizing)
PVI.V6-3
PVI.V6-12
Weight loss (% of starting weight)
Survival (%)
Days post infection
WT
LALA
LALAPG
Negative
Uninfected
PVI.V5-1 WT
PVI.V5-1 LALA
PVI.V5-1 LALAPG

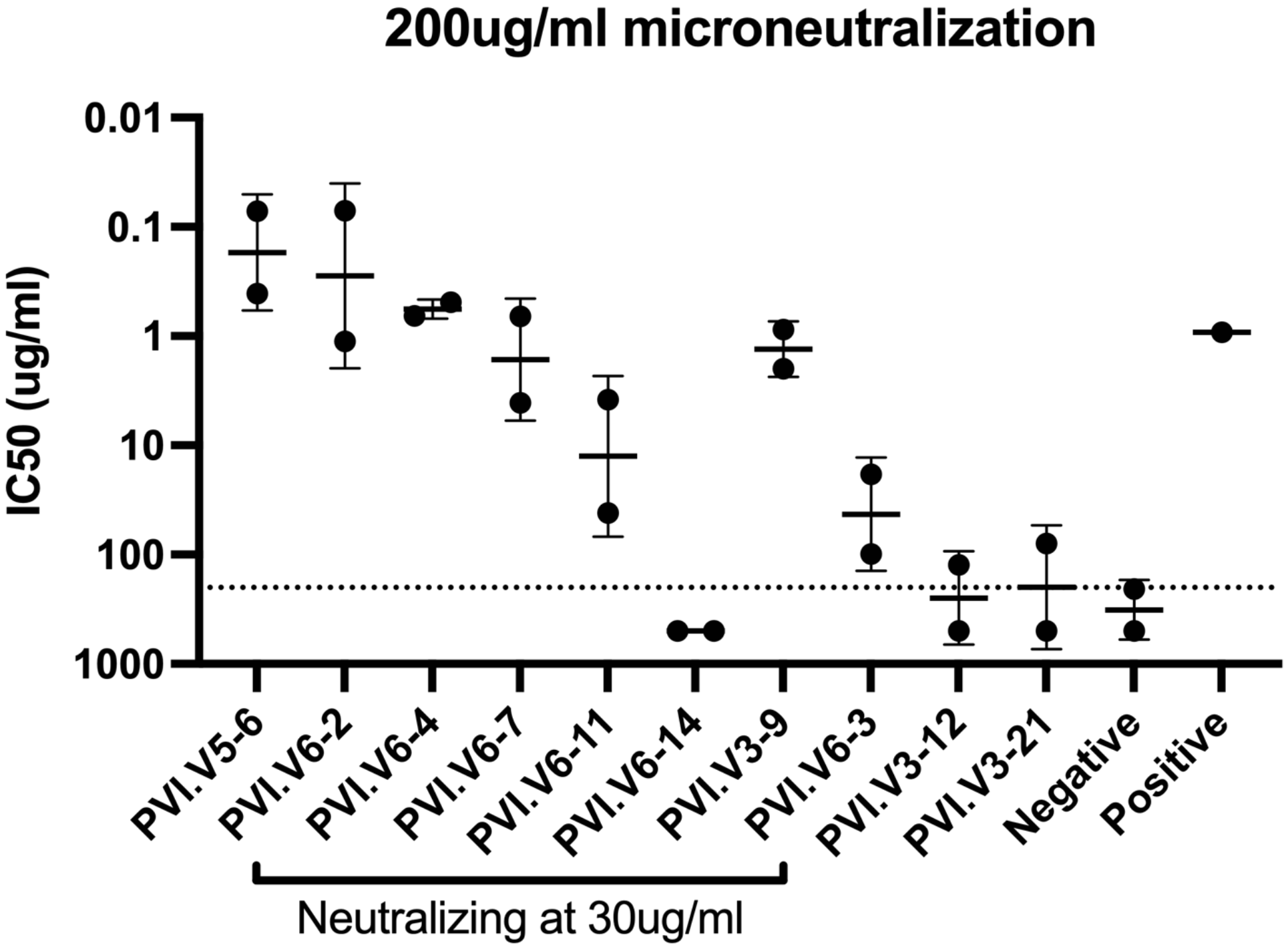
200ug/ml microneutralization
IC50 (ug/ml)
0.01
0.1
1
10
100
1000
PVI.V5-6
PVI.V6-2
PVI.V6-4
PVI.V6-7
PVI.V6-11
PVI.V6-14
PVI.V3-9
PVI.V6-3
PVI.V3-12
PVI.V3-21
Negative
Positive
Neutralizing at 30ug/ml

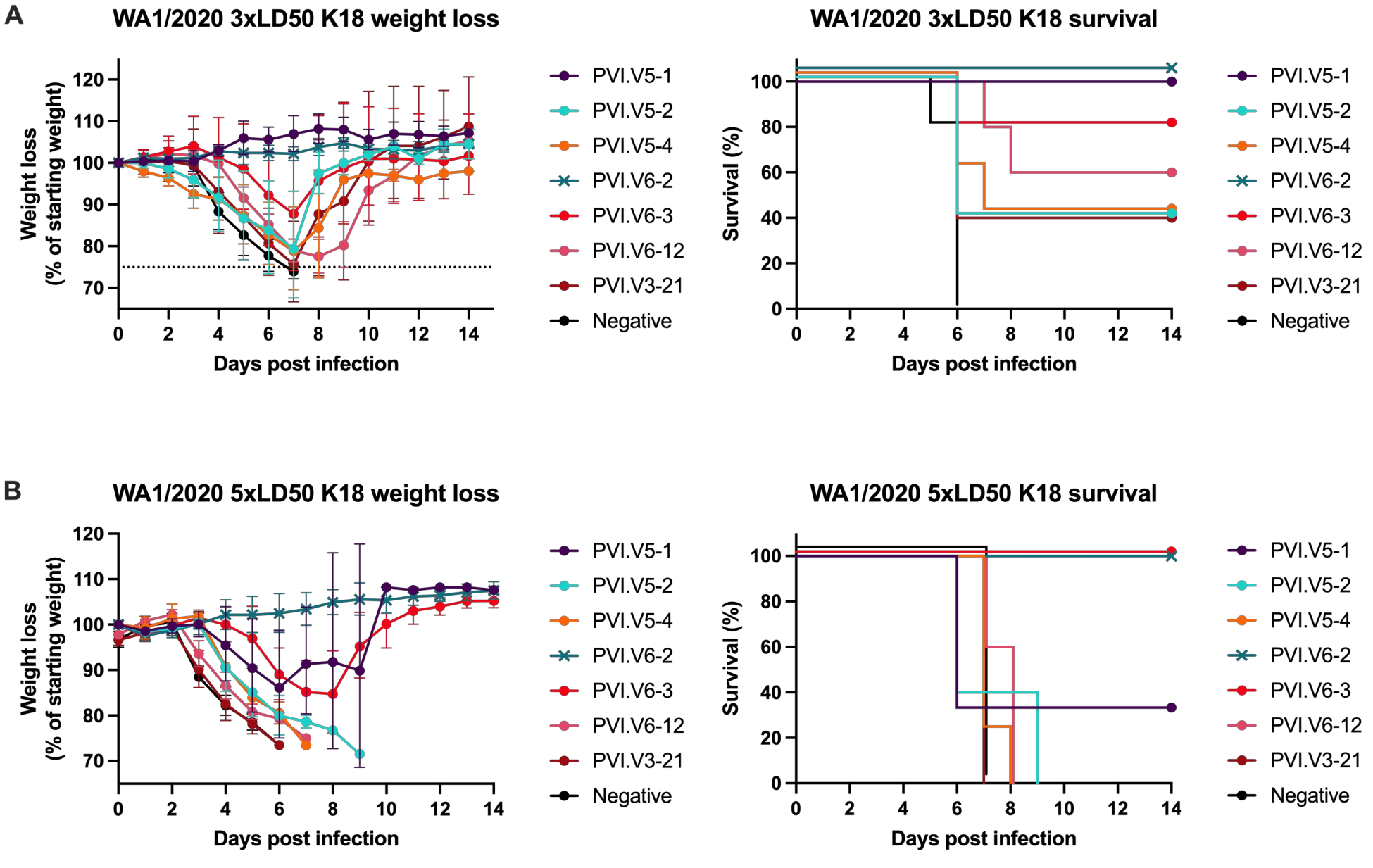
A
WA1/2020 3xLD50 K18 weight loss
Weight loss
(% of starting weight)
Days post infection
WA1/2020 3xLD50 K18 survival
Survival (%)
Days post infection
PVI.V5-1
PVI.V5-2
PVI.V5-4
PVI.V6-2
PVI.V6-3
PVI.V6-12
PVI.V3-21
Negative
B
WA1/2020 5xLD50 K18 weight loss
Weight loss
(% of starting weight)
Days post infection
WA1/2020 5xLD50 K18 survival
Survival (%)
Days post infection
PVI.V5-1
PVI.V5-2
PVI.V5-4
PVI.V6-2
PVI.V6-3
PVI.V6-12
PVI.V3-21
Negative

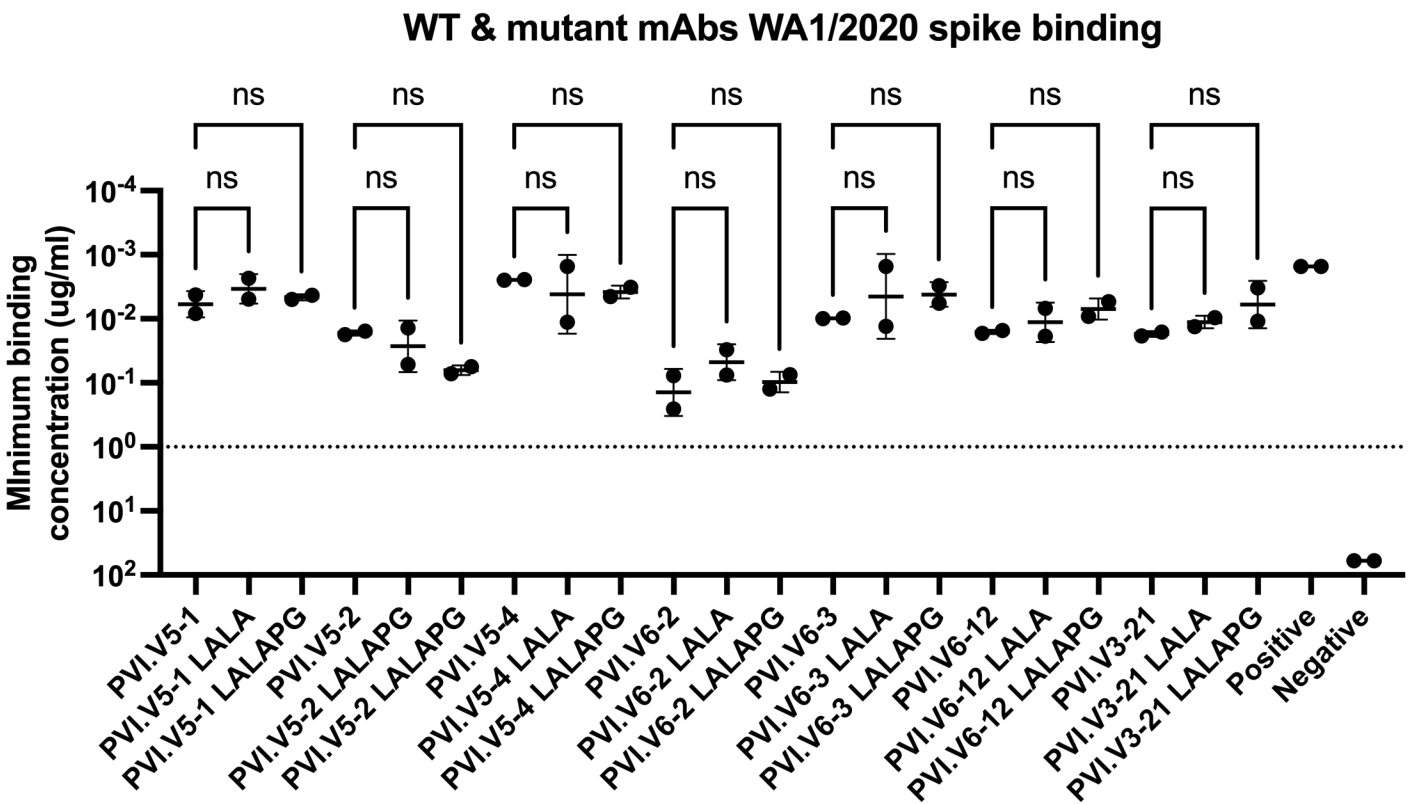
WT & mutant mAbs WA1/2020 spike binding
Minimum binding concentration (ug/ml)
10^{-4}
10^{-3}
10^{-2}
10^{-1}
10^{0}
10^{1}
10^{2}
ns
PVI.V5-1
PVI.V5-1 LALA
PVI.V5-1 LALAPG
PVI.V5-2
PVI.V5-2 LALAPG
PVI.V5-2 LALAPG
PVI.V5-4
PVI.V5-4 LALA
PVI.V5-4 LALAPG
PVI.V6-2
PVI.V6-2 LALA
PVI.V6-2 LALAPG
PVI.V6-3
PVI.V6-3 LALA
PVI.V6-3 LALAPG
PVI.V6-12
PVI.V6-12 LALA
PVI.V6-12 LALAPG
PVI.V3-21
PVI.V3-21 LALA
PVI.V3-21 LALAPG
Positive
Negative

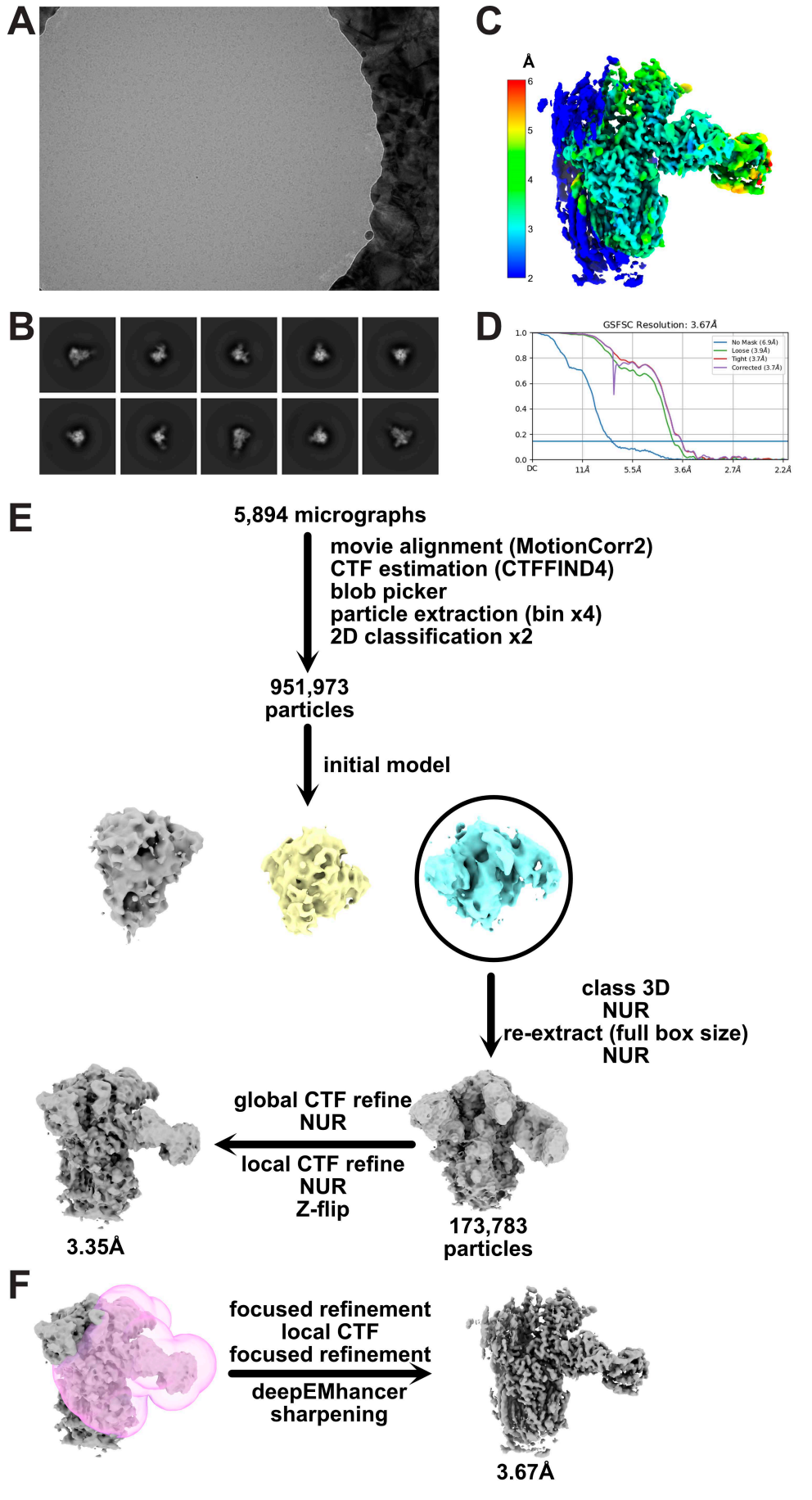
A
C
Å
6
5
4
3
2
B
D
GSFSC Resolution: 3.67Å
No Mask (6.9Å)
Loose (3.9Å)
Tight (3.7Å)
Corrected (3.7Å)
1.0
0.8
0.6
0.4
0.2
0.0
DC
11Å
5.5Å
3.6Å
2.7Å
2.2Å
E
5,894 micrographs
movie alignment (MotionCorr2)
CTF estimation (CTFFIND4)
blob picker
particle extraction (bin x4)
2D classification x2
951,973
particles
initial model
class 3D
NUR
re-extract (full box size)
NUR
global CTF refine
NUR
local CTF refine
NUR
Z-flip
3.35Å
173,783
particles
F
focused refinement
local CTF
focused refinement
deepEMhancer
sharpening
3.67Å